Final Report

Development of catalyst-impregnated metal-foam supported solid oxide electrolysis cell combined with hydrogen separation membrane for hydrogen and syngas production from carbon dioxide and steam integrative with alcohol-assisted methanol synthesis from carbon dioxide and hydrogen

TRF Research Career Development Grant

RSA5880040

Dr. Pattaraporn Kim-Lohsoontorn

Department of Chemical Engineering

Faculty of Engineering

Chulalongkorn University

July 2018

Grant number: RSA5880040

Final Report

Development of catalyst-impregnated metal-foam supported solid oxide electrolysis cell combined with hydrogen separation membrane for hydrogen and syngas production from carbon dioxide and steam integrative with alcohol-assisted methanol synthesis from carbon dioxide and hydrogen

Dr. Pattaraporn Kim-Lohsoontorn Department of Chemical Engineering
Faculty of Engineering
Chulalongkorn University

Supported by Thailand Research Fund (TRF), Mahidol University and Chulalongkorn University

July 2018

Project Code: RSA5880040

Project Title : Development of catalyst-impregnated metal-foam supported solid oxide electrolysis cell combined with hydrogen separation membrane for hydrogen and syngas production from carbon dioxide and steam integrative with alcohol-assisted methanol synthesis from carbon dioxide and hydrogen

Investigator : Dr. Pattaraporn Kim-Lohsoontorn
Department of Chemical Engineering, Faculty of Engineering, Chulalongkorn University

E-mail Address : Pattaraporn.K@chula.ac.th

Project Period : August 2015 - July 2018

Keywords: Solid oxide electrolysis cell, Metal support, Hydrogen separation membrane, Syngas production, Carbon dioxide utilization, Alcohol assisted methanol synthesis

Abstract

There are two platforms of the work from this research: **1)** hydrogen (H_2) and syngas production from steam and carbon dioxide (CO_2) through solid oxide electrolysis cell (SOFC) and **2)** methanol production from carbon dioxide and hydrogen through alcohol-assisted method. The connection between both research platforms is the idea that hydrogen or syngas produced from the first platform can be utilized in the second research platform.

For the first platform, solid oxide electrolysis technology has been developed. The research in this platform has been divided into two focus: **1.1)** improving chemical stability of SOEC and **1.2)** improving fabrication of SOEC. The second research platform presents the correlation between Cu/ZnO catalyst preparation conditions on the catalyst properties and activity in methanol synthesis from CO_2 and H_2.

For the first research platform - improving chemical stability of SOEC, proton conductor material has been synthesized. Effect of strontium and zirconium doped barium cerate on the performance of proton ceramic electrolyser cell for syngas production from carbon dioxide and steam has been studied. Syngas has been produced from carbon dioxide (CO_2) and steam using a proton ceramic electrolyser cell. Proton-conducting electrolytes which exhibit high conductivity can suffer from low chemical stability. In this study, to optimize both proton conductivity and chemical stability, barium cerate and doped barium cerate are synthesized using solid state reaction method: $BaCeO_3$ (BC), $Ba_{0.6}Sr_{0.4}CeO_{3-\alpha}$ (BSC), $Ba_{0.6}Sr_{0.4}Ce_{0.9}Y_{0.1}O_{3-\alpha}$ (BSCY), and $BaCe_{0.6}Zr_{0.4}O_{3-\alpha}$ (BCZ). The BC, BSC, and BSCY are calcined at 1100^{o}C for 2 h and BCZ is calcined at 1300^{o}C for 12 h, respectively. All samples exhibit 100% perovskite and crystallite sizes equal 37.05, 28.46, 23.65 and 17.46 nm for BC, BSC, BSCY and BCZ, respectively. Proton conductivity during steam electrolysis as well as catalytic activity toward the reverse water gas shift reaction (RWGS) is tested between 400 and 800^{o}C. The conductivity increases with temperature and the values of activation energy of conduction are 64.69, 100.80, 103.78 and 108.12 kJ mol^{-1} for BSCY, BC, BSC, and BCZ, respectively. It is found that although BCZ exhibits relatively low conductivity, the material provides the highest CO yield at 550-800^{o}C, followed by BSCY, BSC, and BC, correlating

to the crystallite size and BET surface area of the samples. Catalytic activity toward RWGS of composited Cu and electrolytes is also measured. Additional Cu (60 wt.%) significantly increases catalytic activity. The CO yield increases from 3.01% (BCZ) to 43.60% (Cu/BCZ) at 600^{o}C and CO can be produced at temperature below 400^{o}C. There is no impurity phase detected in BCZ sample after exposure to CO_2-containing gas mixture (600^{o}C for 5 h) while CeO_2 phase is detected in BSC and BSCY and both CeO_2 and BaO are observed in BC sample.

For the second research platform - improving fabrication of SOEC, the effect of sintering additives (NiO, Co_2O_3, and ZnO) on the performance of barium-cerate-based solid oxide electrolysis cell (SOEC) is investigated. The performance of the SOEC with different sintering additives is determined in terms of relative density, electrochemical performance, and catalytic activity toward reverse water gas shift reaction. $BaCeO_3$ (BC) and $BaCe_{0.9}Gd_{0.1}O_{3-\delta}$ (BCG) are synthesized using conventional precipitation method, comparing to ultrasonic-assisted precipitation. The sintering additives promote both densification and grain growth. The relative density of the BCG without sintering additive is 69% while that of the BCG with 1 wt.% of Co_2O_3, NiO and ZnO is 95%, 95% and 88%, respectively. The SEM images indicate that the BCG with sintering additives exhibits dense grains with relatively large grain size. Although the BGC with NiO and Co_2O_3 exhibit maximum relative density, the sample with ZnO shows relatively highest conductivity with the lowest activation energy of conduction and the sample with NiO provides the largest CO yield and CO_2 conversion. The activation energy of conduction is found to be 375.41, 70.06, 66.86 and 61.80 kJmol^{-1} for BCG, BCG with 1 wt.% Co_2O_3, NiO and ZnO, respectively. The BCG with 1 wt.% NiO provides the highest CO_2 conversion and CO yield at temperature below 700^{o}C (62% CO_2 conversion and 32% CO yield at 700^{o}C). Temperature program of oxidation (TPO) reveals that carbon deposition can cause the low CO yield at the operating temperature above 700^{o}C.

For the second research platform – synthesize of methanol from CO_2 and H_2 through alcohol assisted method, CuO/ZnO catalysts are synthesized using a co-precipitation method with different precipitation temperatures (298-353 K) and pH values (5-9). A conventional precipitation is compared to an ultrasonic-assisted precipitation at

each precipitating temperature. Methanol is directly synthesized from CO_2 and H_2 (1:3 mol ratio) through an alcohol-assisted reaction (423 K, 5 MPa, 24 h) by using different alcohols (ethanol, propanol and butanol) as a medium. There are two parts for the challenge of this research, including the preparation of CuO/ZnO catalysts using an ultrasonic-assisted precipitation and, methanol synthesis through an alcohol-assisted method. It is found that the precipitation temperature and pH value significantly affect the catalyst properties and the reaction activity. An ultrasonic irradiation helps facilitate the crystalline phase formation and decrease precipitation temperature. The highest yield of methanol is obtained when CuO/ZnO is precipitated at 333 K from the conventional precipitation (31%) while it is at 313 K from the ultrasonic-assisted precipitation (32%). In addition, the different type of alcohol strongly affects methanol yield and CO_2 conversion. The use of larger alcohol molecules offers higher CO_2 conversion but lower methanol yield.

Table of content

Principle investigation (PI)

Name (PI)	Ms. Pattaraporn Kim-Lohsoontorn (นางภัทรพร คิม)
Qualification	Ph.D.
Position	Assistant Professer
Address	Department of Chemical Engineering, Mahidol University, Nakorn Pathom 73170, Thailand
Telephone	(02) 8892138 Ext 6122
Facsimile	(02) 02-8892138 Ext 6129
Email	pattaraporn.kim@mahidol.ac.th
Responsibility	Project leader
Working hour	20 hr/week

Research area / sub area of this project

Chemical Reaction Engineering, Applied Catalysis, Fuel Processing Technology, Electrochemical engineering

Keywords

Solid oxide electrolysis cell, Metal support, Hydrogen separation membrane, Syngas production, Carbon dioxide utilization, Alcohol assisted methanol synthesis

Total Budget 1,500,000 baht

Project duration 3 years

Abstract

There are two platforms of the work from this research: **1)** hydrogen (H_2) and syngas production from steam and carbon dioxide (CO_2) through solid oxide electrolysis cell (SOFC) and **2)** methanol production from carbon dioxide and hydrogen through alcohol-assisted method. The connection between both research platforms is the idea that hydrogen or syngas produced from the first platform can be utilized in the second research platform.

For the first platform, solid oxide electrolysis technology has been developed. The research in this platform has been divided into two focus: **1.1)** improving chemical stability of SOEC and **1.2)** improving fabrication of SOEC. The second research platform presents the correlation between Cu/ZnO catalyst preparation conditions on the catalyst properties and activity in methanol synthesis from CO_2 and H_2.

For the first research platform - improving chemical stability of SOEC, proton conductor material has been synthesized. Effect of strontium and zirconium doped barium cerate on the performance of proton ceramic electrolyser cell for syngas production from carbon dioxide and steam has been studied. Syngas has been produced from carbon dioxide (CO_2) and steam using a proton ceramic electrolyser cell. Proton-conducting electrolytes which exhibit high conductivity can suffer from low chemical stability. In this study, to optimize both proton conductivity and chemical stability, barium cerate and doped barium cerate are synthesized using solid state reaction method: $BaCeO_3$ (BC), $Ba_{0.6}Sr_{0.4}CeO_{3-\alpha}$ (BSC), $Ba_{0.6}Sr_{0.4}Ce_{0.9}Y_{0.1}O_{3-\alpha}$ (BSCY), and $BaCe_{0.6}Zr_{0.4}O_{3-\alpha}$ (BCZ). The BC, BSC, and BSCY are calcined at 1100^{o}C for 2 h and BCZ is calcined at 1300^{o}C for 12 h, respectively. All samples exhibit 100% perovskite and crystallite sizes equal 37.05, 28.46, 23.65 and 17.46 nm for BC, BSC, BSCY and BCZ, respectively. Proton conductivity during steam electrolysis as well as catalytic activity toward the reverse water gas shift reaction (RWGS) is tested between 400 and 800^{o}C. The conductivity increases with temperature and the values of activation energy of conduction are 64.69, 100.80, 103.78 and 108.12 kJ mol^{-1} for BSCY, BC, BSC, and BCZ, respectively. It is found that although BCZ exhibits relatively low conductivity, the material provides the highest CO yield at 550-800^{o}C, followed by BSCY, BSC, and BC, correlating

to the crystallite size and BET surface area of the samples. Catalytic activity toward RWGS of composited Cu and electrolytes is also measured. Additional Cu (60 wt.%) significantly increases catalytic activity. The CO yield increases from 3.01% (BCZ) to 43.60% (Cu/BCZ) at 600^{o}C and CO can be produced at temperature below 400^{o}C. There is no impurity phase detected in BCZ sample after exposure to CO_2-containing gas mixture (600^{o}C for 5 h) while CeO_2 phase is detected in BSC and BSCY and both CeO_2 and BaO are observed in BC sample.

For the second research platform - improving fabrication of SOEC, the effect of sintering additives (NiO, Co_2O_3, and ZnO) on the performance of barium-cerate-based solid oxide electrolysis cell (SOEC) is investigated. The performance of the SOEC with different sintering additives is determined in terms of relative density, electrochemical performance, and catalytic activity toward reverse water gas shift reaction. $BaCeO_3$ (BC) and $BaCe_{0.9}Gd_{0.1}O_{3-\delta}$ (BCG) are synthesized using conventional precipitation method, comparing to ultrasonic-assisted precipitation. The sintering additives promote both densification and grain growth. The relative density of the BCG without sintering additive is 69% while that of the BCG with 1 wt.% of Co_2O_3, NiO and ZnO is 95%, 95% and 88%, respectively. The SEM images indicate that the BCG with sintering additives exhibits dense grains with relatively large grain size. Although the BGC with NiO and Co_2O_3 exhibit maximum relative density, the sample with ZnO shows relatively highest conductivity with the lowest activation energy of conduction and the sample with NiO provides the largest CO yield and CO_2 conversion. The activation energy of conduction is found to be 375.41, 70.06, 66.86 and 61.80 kJmol^{-1} for BCG, BCG with 1 wt.% Co_2O_3, NiO and ZnO, respectively. The BCG with 1 wt.% NiO provides the highest CO_2 conversion and CO yield at temperature below 700^{o}C (62% CO_2 conversion and 32% CO yield at 700^{o}C). Temperature program of oxidation (TPO) reveals that carbon deposition can cause the low CO yield at the operating temperature above 700^{o}C.

For the second research platform – synthesize of methanol from CO_2 and H_2 through alcohol assisted method, CuO/ZnO catalysts are synthesized using a co-precipitation method with different precipitation temperatures (298-353 K) and pH values (5-9). A conventional precipitation is compared to an ultrasonic-assisted precipitation at

each precipitating temperature. Methanol is directly synthesized from CO_2 and H_2 (1:3 mol ratio) through an alcohol-assisted reaction (423 K, 5 MPa, 24 h) by using different alcohols (ethanol, propanol and butanol) as a medium. There are two parts for the challenge of this research, including the preparation of CuO/ZnO catalysts using an ultrasonic-assisted precipitation and, methanol synthesis through an alcohol-assisted method. It is found that the precipitation temperature and pH value significantly affect the catalyst properties and the reaction activity. An ultrasonic irradiation helps facilitate the crystalline phase formation and decrease precipitation temperature. The highest yield of methanol is obtained when CuO/ZnO is precipitated at 333 K from the conventional precipitation (31%) while it is at 313 K from the ultrasonic-assisted precipitation (32%). In addition, the different type of alcohol strongly affects methanol yield and CO_2 conversion. The use of larger alcohol molecules offers higher CO_2 conversion but lower methanol yield.

Research significance and introduction

Thailand mainly relies on energy from petroleum, including refining or reforming of imported crude oil. Regarding the issue of national energy security as well as increasing price of the oil which is limited resource, an alternative energy technology has gained much interest and urgently required for research and development. Moreover, significant amount of carbon dioxide (CO_2) is being released out of the processes involving energy management and conversion. The global CO_2 emission is at 6.2 trillion tons per year and it tends to increase. The increasing CO_2 concentration in atmosphere was predicted to be 44% from 2006 to 2030 [1]. Carbon capture and sequestration (CCS) has been proposed as a strategy to decrease accumulated CO_2 in the atmosphere. However, the technological challenge is remained as it is not possible to evaluate the impact of storing large amount of CO_2 into uncontrolled undergrounds layers. The leakage of the gas back to the surface is still a concerned.

The importance of this project is to increase national energy security at the same time as solving environmental problem. The strategy is the utilization of CO_2 and water to produce methanol. It is well known that methanol (CH_3OH) is an important precursor to the production of many chemicals such as formaldehyde, acetic acid, methyl tertiary butyl ether (MTBE) or even DME. These all chemicals are necessary for other industrial sectors such as transportation and construction. Moreover, methanol is a

reactant in the process of bio-diesel production which is one of the alternative fuels, strongly driven in Thailand. However, there is no methanol production process in country at the present. This results a high imported rate of methanol each year. The methanol consumption in Thailand is varied with the production rate of bio-diesel which is 2.5 million liters per day [Department of alternative energy development and efficiencies, Ministry of energy]. For the global figure, methanol consumption is 65 million ton per year [2] and 75 percent of methanol is synthesized from natural gas or coal which results in a liberation of CO_2 from the processes [3-15].

Methanol is generally synthesized through thermochemical process that syngas ($CO+H_2$) was used as a precursor. However, syngas is normally derived from natural gas which is limited natural resources and the reforming process results in CO_2 emission. Apart from thermochemical process, syngas can be synthesized using electrochemical process of co-electrolysis between steam and CO_2. If the electricity required for this process is derived from renewable energy sources, then this represents a low (or zero) carbon route to syngas production. The important advantage is producing very pure H_2 and CO without the need for further processing to remove impurities that would negatively impact system performance and durability. Relatively high operating temperatures can reduce the electrical energy requirement of the electrolysis process and, thereby, the cost of production. Operating temperatures improve the electrode kinetics and reduce the SOEC electrolyte resistance, leading to lower losses in cell

performance. If waste heat from power stations or other industrial processes can be used to sustain the electrolyser operation, SOECs have the potential to generate H_2 at a significantly higher efficiency compared to the low temperature electrolysers.

Reference

[1] Shamsul N.S, Kamarudin S.K, Rahman N.A, Kofli N.T. An overview on the production of bio-methanol as potential renewable energy. Renewable and Sustainable Energy Reviews. 2014; 33: 578–588.

[2] Hori Y., Wakebe H., Tsukamoto T., Koga O. Electrocatalytic process of CO selectivity in electrochemical reduction of CO_2 at metal-electrodes in aqueous-media. Electrochim Acta. 1994; 39: 1833-1839.

[3] Toyir J, De lPPR, Fierro JLG, Homs N. Highly effective conversion of CO_2 to methanol over supported and promoted copper-based catalysts: influence of methanol over supported and promoter. Appl Catal B 2001; 29: 207-215.

[4] Toyir J, Ramirez dIPP, Fierro JLG, Homs N. Catalytic performance for CO_2 conversion to methanol of gallium-promoted copper-based catalysts: influence of metallic precursors. Appl Catal B 2001; 34: 255-266.

[5] Liu J, Shi J, He D, Zhang Q, Wu X, Liang Y. Surface active structure of ultra-fine Cu/ZrO_2 catalysts used for the CO_2+H_2 to methanol reaction. Appl Catal A 2001; 218: 113-119.

[6] Guo X, Mao D, Wang S, We G, Lu G. Combustion synthesis of CuO-ZnO-ZrO_2 catalysts for the hydrogenation of carbon dioxide to methanol. Catal Commun 2009; 10: 1661-1664.

[7] Raudaskoski R, Niemelae MV, Keiski RL. The effect of ageing time on co-precipitated $Cu/ZnO/ZnO_2$ catalysts used in methanol synthesis from CO_2 and H_2. Top Catal 2007; 45: 57-60

[8] Sloczynski J, Grabowski R, Olszewski P, Kozlowska A, Stoch J, Lachowska M. Effect of metal oxide additive and stability of $Cu/ZnO/ZrO_2$ catalysts in the synthesis of methanol from CO_2 and H_2. Appl Catal A 2006; 210: 127-137.

[9] Sloczynski J, Grabowski R, Kozlowska A, Olszewski P, Stoch J, Skrzypek J. Catalytic activity of the $M/(ZnO\ ZrO_2)$ system (M = Cu, Ag, Au) in the hydrogenation of CO_2 to methanol. Appl Catal A 2004; 278: 11-13.

[10] Liu X-M, Lu GQ, Yan Z-F. Nanocrystalline zirconia as catalyst support in methanol synthesis. Appl Catal A 2005; 279: 241-245.

[11] Chinchen GC, Spencer MS, Waugh KC, Whan DA. Promotion of methanol synthesis and the water-gas shift reactions by adsorbed oxygen on supported copper catalysts. J Chem Soc Faraday Trans 1: Phys Chem Condens Phases 1987; 83: 2193-2212.

[12] Joo O-S, Jung K-D, Moon I, Rozovskii AY, Lin GI, Han S-H. Carbon dioxide hydrogenation to form methanol via a reverse-water-gas-shift reaction. Ind Eng Chem Res 1999; 38: 1808-1812.

[13] Chinchen GC, Spencer MS Chinchen GC, Waugh KC, Whan DA. The activity and state of copper surface in methanol synthesis catalyst. Appl Catal 1986; 25: 101-107.

[14] Satio M, Murata K. Development of high performance Cu/ZnO-based catalysts in methanol synthesis and the water-gas-shift reaction. Catal Surv Asia 2004; 8: 285-294

[15] Wu J. Satio M, Takeuchi M, Watanabe T. The stability of Cu/ZnO-based catalysts in methanol synthesis from a CO_2-rich feed and from CO-rich feed. Appl Catal A: Gen 2001; 218: 235-240.

Research objective

1. To develop the scientific knowledge for the production of methanol from carbon dioxide and water through an electrochemical process in solid oxide electrolysis cell (SOEC) connected with a thermochemical process
2. To develop the scientific knowledge for the production of methanol from carbon dioxide and water through an intermediated-temperature and pressurized solid SOEC in a single step
3. To achieve a prototype of proton-conducting SOEC for methanol production through a study of proper ceramics, synthesis method, and sintering additives

Research output

Research outputs over the three-year project are as followed:

Output	Number
1. International publications	3
2. Bachelor degree graduate	14
3. Master degree graduate	3
4. Prototype reactor for methanol synthesis	1
5. Prototype of proton-conductor SOFC	2

List of publication in international journal is as followed:

Year	Publication	Quartile
2018	Likhittaphon S, Pukkrueapun T, Seeharaj P, Wetwathana Hartley U, Laosiripojana N, Kim-Lohsoontorn P, The effect of sintering additives on the performance of barium cerate based solid oxide electrolysis cell. Fuel Processing Technology. 2018; 173: 119-125.	Q1
2018	Effect of CuO/ZnO catalyst preparation condition on alcohol-assisted methanol synthesis from carbon dioxide and hydrogen, Likhittaphon S, Panyadee R, Fakyam W, Charojrochkul S, Sornchamni, Laosiripojana N, Assabumrungrat S, Kim-Lohsoontorn P. International journal of hydrogen energy. 2018. In Press.	Q1
2018	Sarabut J, Charojrochkul S, Sornchamni T, Laosiripojana N, Assabumrungrat S, Wetwattana-Hartely U, Kim-Lohsoontorn P. Effect of strontium and zirconium doped barium cerate on the performance of proton ceramic electrolyser cell for syngas production from carbon dioxide and steam. International Journal of Hydrogen Energy. 2018 (Accepted)	Q1

Research platform 1

Hydrogen and syngas production from steam and carbon dioxide through solid oxide electrolysis cell (SOEC)

1.1 Effect of strontium and zirconium doped barium cerate on the performance of proton ceramic electrolyser cell for syngas production from carbon dioxide and steam

1.1.1 Research platform 1.1 - Introduction

Significant amount of carbon dioxide (CO_2) has been released from processes involving energy conversion. The emission enhances the green-house effect and contributes to global climate change which could endanger environment and mankind. Consequently, CO_2 utilization as a carbon source for the production of fuels and chemicals has gained much interest. Proton ceramic electrolyser cells (PCECs) can convert CO_2 and steam into syngas (hydrogen (H_2) and carbon monoxide (CO)) which is known as important precursor for industrial chemicals such as higher olefin and alcohols [1-5]. With CO_2 and H_2O as a feed, H_2 is produced through steam electrolysis reaction (equations (1)-(3)). Hydrogen then further reacts with CO_2 to form CO. The reverse water gas shift (RWGS) reaction provides syngas (H_2 and CO) as a product through equation (4).

Electrochemical reaction:

Anode: $H_2O \rightarrow 2H^+ + 2e^- + ½\ O_2$ (1)

Cathode: $2H^+ + 2e^- \rightarrow H_2$ (2)

Overall reaction: $H_2O \rightarrow H_2 + 1/2O_2$ (3)

Thermochemical reaction:

RWGS: $CO_2 + H_2 \rightarrow H_2O + CO$ (4)

The electrolyte of an electrolyser can be oxygen-ion (O2-) conductor or proton (H^+) conductor. In theory, proton exhibits much smaller ionic radius comparing to oxygen-ion. Therefore, the mobility is relatively higher, leading to higher conductivity and the cell performance [6-9]. Proton-conducting electrolytes also permit a significant decrease in operating temperature (400-700°C), resulting in increasing system robustness and reducing system cost [10, 11].

However, the materials which exhibit high proton conductivity often suffer from poor chemical stability when being exposed to CO_2-containing gas. Barium cerate ($BaCeO_3$) is known to exhibit high proton conductivity but low chemical stability against CO2 [9, 12-19] while barium zirconate ($BaZrO_3$) shows relatively higher chemical stability but lower proton conductivity [14, 15, 20-22]. Therefore, zirconium doped barium cerate

(BCZ) has been used as an electrolyte and composites with metal as an electrode [23-26]. Doping trivalent such as Y^{3+}, Yb^{3+}, Nd^{3+} and Gd^{3+} into BCZ to achieve higher conductivity was also reported [8, 11, 13, 14, 16, 17, 20, 21, 25, 29]. Strontium cerate ($SrCeO_3$) exhibits conductivity and chemical stability against CO_2 and the performance lies between $BaCeO_3$ and $BaZrO_3$ [8, 22, 29]. Therefore, strontium doped barium cerate (BSC) and the BSC with trivalent doping have also been investigated [8, 15, 18, 22, 27-29].

The objective of this study is to optimize both proton conductivity and chemical stability by using a combination of the $BaCeO_3$ (exhibiting high proton conductivity), $SrCeO_3$, and $BaZrO_3$ (exhibiting high chemical stability). The perovskite compositions of strontium doped barium cerate ($Ba_{0.6}Sr_{0.4}CeO_{3-\alpha}$, BSC), and zirconium doped barium cerate ($BaCe_{0.6}Zr_{0.4}O_{3-\alpha}$, BCZ) have been synthesized. To achieve higher conductivity, Y^{3+} was also doped into SCB structure ($Ba_{0.6}Sr_{0.4}Ce_{0.9}Y_{0.1}O_{3-\alpha}$, BSCY). The electrochemical performance and catalytic activity of the samples were investigated. The catalytic activity of electrode and electrolyte materials toward RWGS reaction was discussed. The chemical stability of prepared samples when being exposed to CO_2 was also measured.

1.1.2 Research platform 1.1 – Experimental

1.1.2.1 Research platform 1.1 – Sample preparation

The BC, BSC, BSCY, and BCZ were prepared using solid state reaction method. Stoichiometric amounts of $BaCO_3$ (In house), CeO_2 (99.95%, Sigma Aldrich $SrCO_3$ (99.9%, Sigma Aldrich,), ZrO_2 (99.0%, Kanto Chemical Company), Y_2O_3 (99.99%, Sigma Aldrich), were used as precursors. The precursors were mixed by ball milling for 24 h using zirconia balls having 5 mm and 10 mm diameter and ethanol (95%, Sigma Aldrich) as a medium, followed by drying in oven at 105 ^oC for 24 h and calcination at 1100^oC for 2 h (BC, BCS and BCSY) and 1300^oC for 12 h (BCZ).

To fabricate a button-type electrolyser, prepared powder of 3 g was pressed into a pellet at 1500 psi for 30 seconds and sintered at 1450^oC for 15 h. The sintering temperature and time could be reduced if sintering aid is added [30]. However, sintering aid was not applied in the sample, not to interfere the experimental results in this study. The relative density of fabricated cell was calculated and the method of calculation can be referred in our previous work [30]. The sintered cell was then coated by silver conductive paste (Sigma-Aldrich). The coated pellet was fired at 900^oC for 2 h, giving an electrode layer with an area of 0.785 cm^2 and a thickness of ~30 μm.

1.1.2.2 Research platform 1.1 – Characterization

The X-ray diffraction (XRD) was used (BRUKER model D8 advance, using Kα radiation of Cu) with scanned 2θ between 10° – 80°. The phase was identified by comparing with JCPDS database. Crystallize size (d) was calculated using Scherrer equation:

$$d=0.9\lambda/(\beta FWHM\ Cos(\theta)) \quad (5)$$

where λ is the wavelength (1.54 Å), βFWHM is the full width for the half-maximum intensity of main peaks (FWHM), and θ is diffraction angle.

%Perovskite was determined from equation (6) through a measuring of the intensity of XRD major peaks.

$$\%Perovskite=(\sum(I_{perovskite})/I_T\ x100 \quad (6)$$

where $I_{perovskite}$ is the intensity of perovskite peaks, I_T is the total intensity of perovskite peaks and impurity peaks.

Surface area of the materials was measured through N_2 adsorption and desorption (Autosorb 1-AG, Quantachrome).

1.1.2.3 Research platform 1.1 – Electrochemical performance measurement

The electrochemical performance measurement was carried out between 400-800^{o}C with humidified H_2/N_2 feed. Single cell polarisation curves were generated using linear sweep current techniques to obtain a V/I curve. A potentiostat (Metrohm Autolab, Netherlands) was used to control the voltage between open circuit voltage (OCV) and 1.5 V with a scan rate of 20 mV/s. Platinum wires were attached to the cell for an electrical connection. The cell was placed in a cell holder which was sealed using glass sealant (Untra-Temp 516, Aramco, USA) to separate the gas environment of two electrode chambers. A vertical furnace (Chavachot, Thailand) was used to control the temperature of the test rig. The test system allowed variable gas compositions of steam, and H¬2 (20%H_2O, 24%H_2 and 56%N_2, 100 ml min-1 total flow rate) to be introduced to the electrode. After passing through flow controllers, the H_2 line passes through the humidifier, which is a bubble column situated inside a thermocirculator bath, to saturate the gas with water.

The value of activation energy (E_a) of conductivity can be related to proton conductivity. Activation energy of conduction decreases when proton conductivity increases. Proton conductivity was calculated using equation (7) and activation energy of conduction was calculated using Arrhenius, equation (8):

$$\sigma = LI/VA \qquad (7)$$

$$\sigma = A/T\ e^{((-Ea)/RT)} \quad (8)$$

When σ is proton conductivity (S cm^{-1}); L is the sample cell thickness (cm); I is a current (A); V is a controlled voltage (V); A is an electrode area (cm^2); T is temperature (K); E_a is an activation energy of conductivity (J mol^{-1}); and R is gas constant (8.314 J K^{-1} mol^{-1})

1.1.2.4 Research platform 1.1 – Catalytic activity performance test

The activity toward reverse water gas shift reaction was tested between 400-800^oC with an interval of 50^oC, using a heating rate of 10^oC min-1. The electrolyte powders were sieved to 70 -100 nm. After that, 0.1 g of an electrolyte power was packed inside a 4 mm inner-diameter quartz tube reactor. A gas mixture of 10%CO_2, 10%H_2 and 80%Ar_2 (100 mL min^{-1} total flow rate) was fed to the reactor. Out-gas products were detected by gas chromatography (GC-2014, Shimadzu CORP).

Composited Cu and electrolytes were also tested. The electrolyte power was mixed with CuO (98% CuO, Sigma Aldrich) at a proper ratio to obtain a ratio of Cu to electrolyte at a 60:40 wt.%. Mixed powder were sieved to 70 -100 nm and 0.1 g of samples were used for catalytic activity test. The samples were reduced in-situ at 350ºC for 40 min in a flow of a 10% H_2/Ar mixture (20 mL min-1) prior to the reaction. The catalytic activity toward reverse water gas shift reaction was then performed.

1.1.2.5 Research platform 1.1 – Chemical stability test

The chemical stability of the sintered pellets was carried out in CO_2-containing environment. The sintered pellet was placed in the cell holder and the cell ridge was sealed using glass sealant (Ultra-Temp 516, Aramco, USA). A vertical furnace (Chavachot, Thailand) was used to control the temperature of the rig. The cell was exposed to 10%CO_2, 30%H_2 and 60%N_2 (300 ml min-1 total flow rate) at 600^{o}C for 5 h. The phases of the sintered pellets after CO_2 exposure were analyzed using XRD.

The Goldschmidt tolerance factor (τ) was used to predict a distortion of a crystal structure and was related to chemical stability of a perovskite structure [23]. The factor can be calculated using equation (9), as result τ = 1 is for a perfect cubic perovskite.

$$\tau = (r_A + r_O)/(\sqrt{2}\,(r_B + r_O)) \qquad (9)$$

where r_A is the ionic radius of the A site which is Ba^{2+} (1.35Å) or Sr^{2+} (1.18Å); r_B is the ionic radius of the B site which are Ce^{4+} (0.87Å), Zr^{4+} (0.72Å), or Y^{3+} (0.9Å); and r_O is the ionic radius of the oxygen O^{2-} (1.40 Å).

1.1.3 Research platform 1.1 – Results and discussion

1.1.3.1 Research platform 1.1 – Characterization

The XRD patterns of all prepared electrolyte poweders were shown in Fig. 1. All samples exhibited perovskite structure (JCPDS 82-2425). There was no impurity phase detected and 100% perovskite was obtained in all prepared powder. The crystallite sizes calculated from XRD patterns are also presented in Table 1. They were 37.05, 28.46, 23.65 and 17.46 nm for BC, BSC, BSCY, and BCZ, respectively. The crystallite sizes of the BCZ and the BSC are smaller than that of the BC due to a Zr^{4+} substitution at Ce^{4+} sites and a Sr^{2+} substitution at Ba^{2+} sites, resulting in a decreased unit cell volume. Relatively smaller size of Zr^{4+} ions (radius of 0.72 Å) substituted the larger Ce^{4+} ions (radius of 0.87 Å) and Sr^{2+} ions (radius of 1.18 Å) substituted Ba^{2+} ions (radius of 1.35 Å), respectively.

Table 1 %Perovskite, crystallite size, relative density, tolerance factor, and surface area of synthesized electrolyte powder and surface area of composited Cu/electrolytes

	BC	BSC	BSCY	BCZ
% Perovskite	100	100	100	100
Crystallize size (nm)	37.05	28.46	23.65	17.46
Relative density (%)	70.15	85.99	87.22	56.68
Tolerance factor (τ)	0.857	0.835	0.834	0.880

	BC	BSC	BSCY	BCZ
BET surface area ($m^2\ g^{-1}$)	2.53	3.01	2.07	3.53
BET surface area ($m^2\ g^{-1}$)	Cu/BC 8.60	Cu/BSC 9.10	Cu/BSCY 10.85	Cu/BCZ 15.02

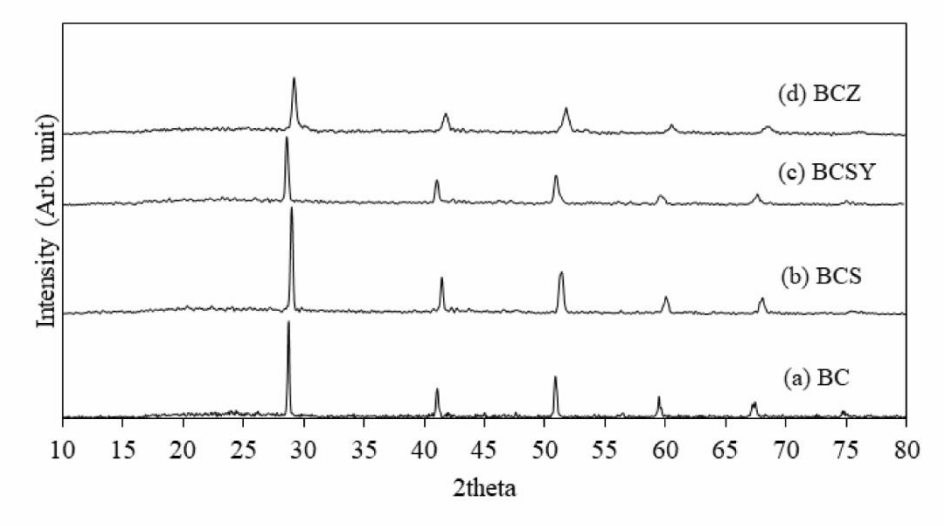

Figure 1 The XRD patterns of synthesized electrolytes: **(a)** barium cerate (BC), **(b)** strontium doped barium cerate (BCS), **(c)** yttrium and strontium doped barium cerate (BCSY), and **(d)** zirconium doped barium cerate (BCZ)

When barium cerate was doped by Zr^{4+} ions and Sr^{2+} ions, the main peak shifted to a larger diffraction angle due to a decrease in lattice parameters as presented in Fig.2. This result corresponded to other work [14] and confirmed the incorporation of Zr^{4+} ions in the BCZ as well as the Sr^{2+} in the BCS. For the BSCY sample, co-doping Sr

and Y into barium cerate resulted in a shift of main peak to a lower diffreaction angle due to an increase in unit cell volume.

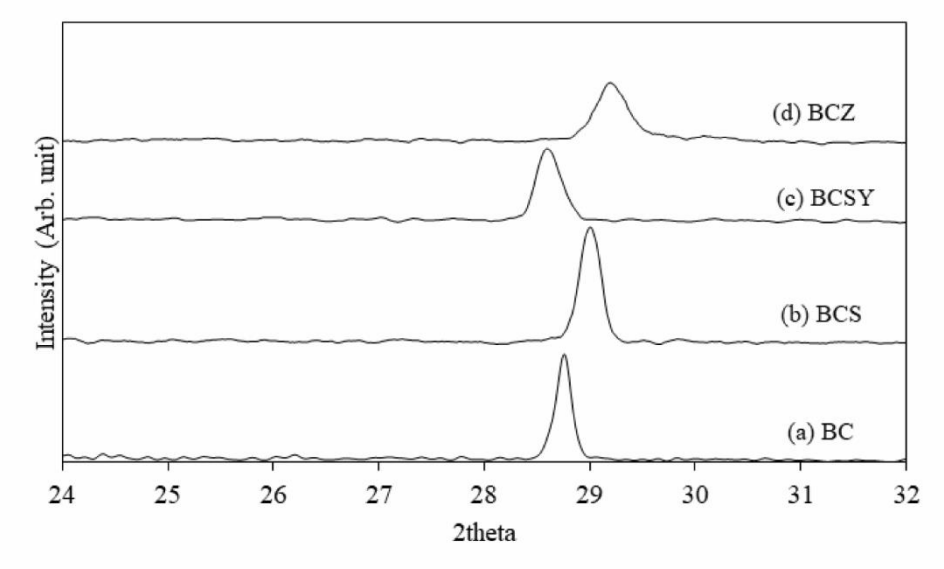

Figure 2 Magnified scale of XRD patterns representing the shift in the main peak of **(a)** barium cerate (BC), **(b)** strontium doped barium cerate (BCS), **(c)** yttrium and strontium doped barium cerate (BCSY), and **(d)** zirconium doped barium cerate (BCZ)

1.1.3.2 Research platform 1.1 – Activation energy of conduction

The synthesized powder was prepared into a pellet and an V/I curve was generated between 400-800ºC. Figure 3 presents the conductivity of electrolyte pellet and calculated activation energy of conduction. It was found that the conductivity increased with temperature and the BSCY pellet exhibited the highest conductivity, followed by BC,

BSC and BCZ, respectively. The activation energy of condcuction was 64.69, 100.80, 103.78 and 108.12 kJ mol-1 for BSCY, BC, BSC, and BCZ, respectively. The H2 production rate was also calculated from current at 1.1 V and 800^{o}C, and the rate was 1.39 x 10^{-8}, 3.38 x 10^{-8}, 6.06 x 10^{-9}, and 1.24 x 10^{-10} mol s^{-1} for BC, BSC, BSCY, and BCZ, respectively.

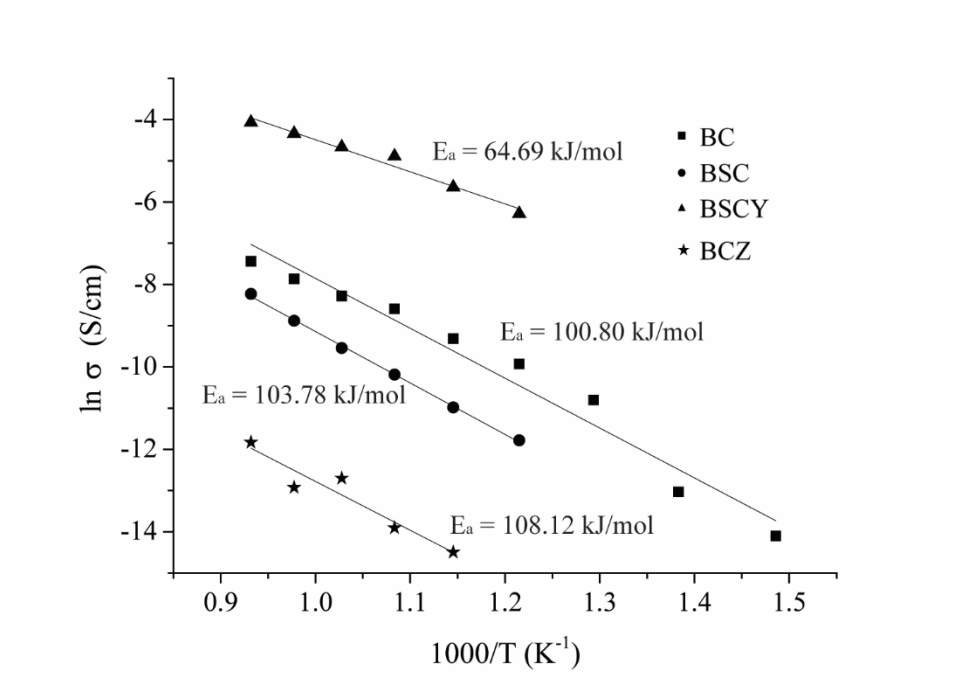

Figure 3 Activation energy of conduction (Ea) of fabricated electrolytes: barium cerate (BC), strontium doped barium cerate (BCS), yttrium and strontium doped barium cerate (BCSY), and zirconium doped barium cerate (BCZ)

The content of barium ion and zirconium ion can affect a proton conductor. It was reported that the conductivity increases with an increasing barium content [32] while the conductivity decreases with an increasing zirconium content [20]. A rare-earth ion dopant also affects $BaCeO_3$ proton conductor [18, 31]. Fu and Weng [31] investigated the

conductivity of various rare-earth ions doped $BaCeO_3$ ($BaCe_{0.9}M_{0.1}O_{2.95}$, M is Gd, Nd, Sm and Y) and $BaCe_{0.9}Y_{0.1}O_{2.95}$ was reported to show relatively higher proton conductivity ($9.20x10^{-3}$ S cm^{-1}) than $BaCeO^3$ ($1.13x10^{-4}$ S cm^{-1}) at 800^oC in 5%H_2-95%Ar while Wang et.al [18] reported that the conductivity of $Ba_{0.6}Sr_{0.4}Ce_{0.8}Y_{0.2}O_{3-\delta}$ is between 2.25 $x10^{-2}$ and $2.5x10^{-2}$ S cm^{-1}.

The % relative density was also calculated from the sintered electrolyte pellets and is presented in Table 1. It was found that the BSCY exhibited the highest %relative density (87.22%), followed by BSC (85.99%), BC (70.15%), and BCZ (56.68%), respectively. The relative density could also affect the electrochemical performance of the electrolyte pellets. It should be noted that the relative density reported in this study was rather low. The relative density of the sample can be related to sinterability which mainly depends on mass transport diffusion mechanism and can be affected by factors such as starting power size, sintering temperature and time, and sintering additive. Although the relative density could be increased by adding a sintering additive [30], it was not applied in this study, not to interfere the experimental results.

Although doping barium cerate with Zr^{4+} and Sr^{2+} slightly increased activation energy of conduction (decreased conductivity), it was found that doping barium cerate with Zr^{4+} or Sr^{2+} significantly improved catalytic activity toward the RWGS reaction and Zr^{4+} dopant also helped improve chemical stability of the cell in CO_2-containing environment (Sections 3.3 and 3.4).

1.1.3.3 Research platform 1.1 – Catalytic activity toward RWGS reaction

The catalytic activity was tested toward the RWGS reaction and the conversion of CO_2 and the yield of CO are presented in Fig. 4(a)-(d). It was found that the CO_2 conversion and the CO yield can be gained at a temperature between 550-800^oC for all electrolyte samples (Figs 4(a) and 4(b)) and at a temperature between 400-800^oC for all composited Cu and electrolyte samples (Figs 4(c) and 4(d)). The catalytic activity increased with increasing temperature. Adding Cu metal significantly increased catalytic activity of the samples and allowed the RWGS reaction to occur at the intermediate temperatures of an electrolyser. This could emphasize an advantage of a cermet type as an electrode for CO_2/H_2O-fed electrolyser. An increase in catalytic performance of Cu/BSCY toward the RWGS reaction is still unclear and requires further experimental investigation. However, the effect of catalyst support on Cu dispersion has been reported in other work [33]. This could be responsible for difference in catalytic performance of the electrolyte samples after adding Cu component.

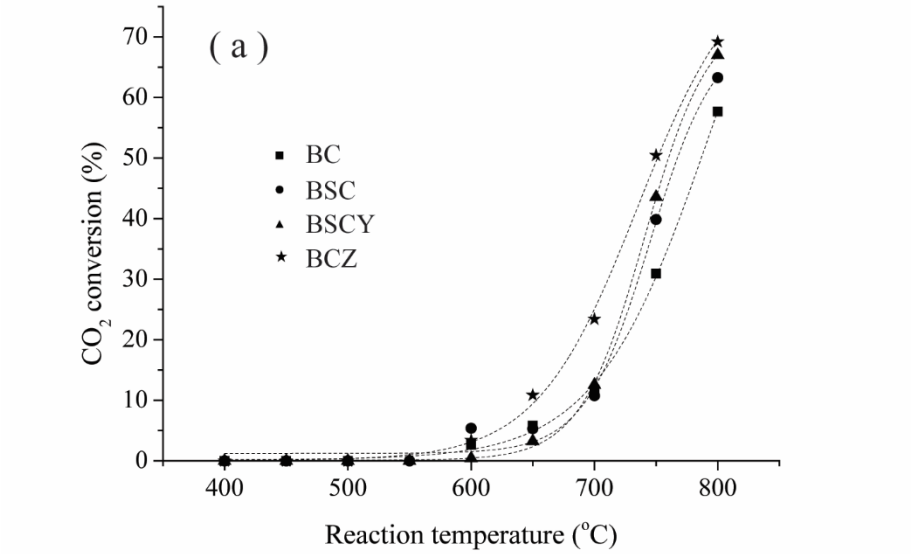
(a)
BC
BSC
BSCY
BCZ
CO_2 conversion (%)
Reaction temperature (°C)
0
10
20
30
40
50
60
70
400
500
600
700
800

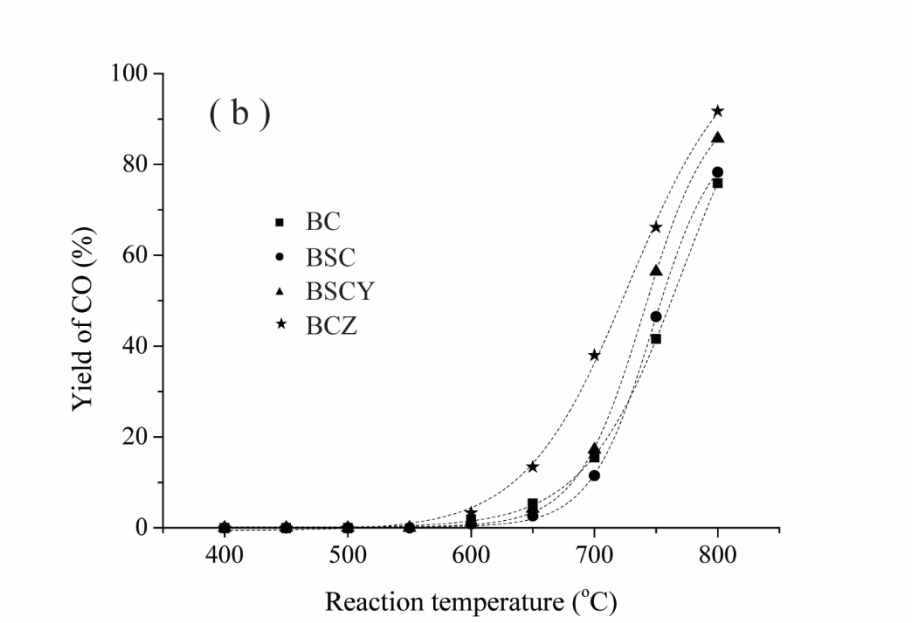
(b)
BC
BSC
BSCY
BCZ
Yield of CO (%)
Reaction temperature (°C)
0
20
40
60
80
100
400
500
600
700
800

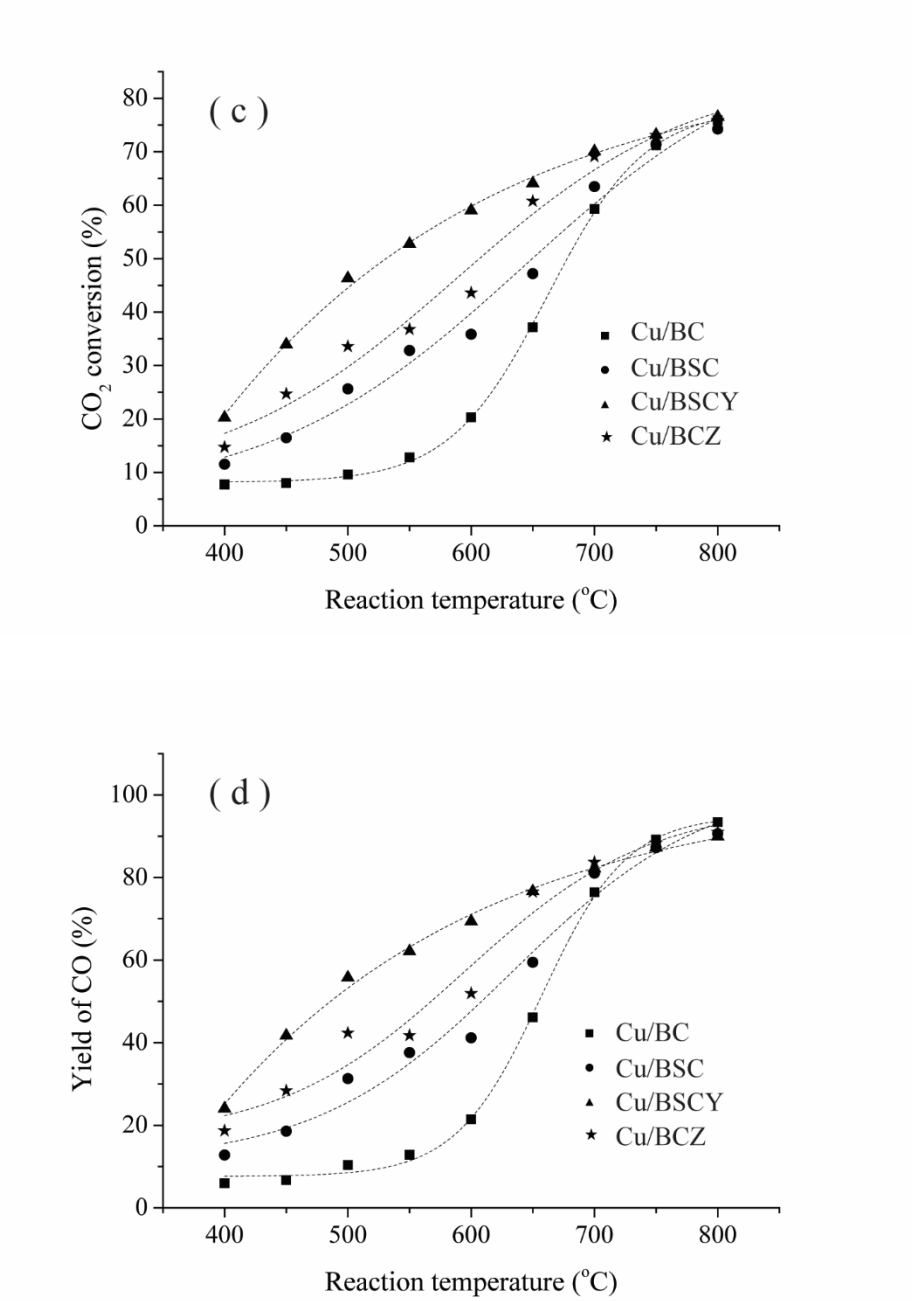

Figure 4 Catalytic activity of electrolytes (BC, BSC, BSCY, and BCZ) and electrode materials (composited Cu/electrolytes) toward the reverse water gas shift (RWGS) reaction: **(a)** CO_2 conversion and **(b)** CO yield when using electrolyte powder as catalyst; **(c)** CO_2 conversion and **(d)** CO yield when using electrode powder as catalyst

An increase in catalytic activity of doped barium cerate when compared to bare barium cerate is not clearly known; however, it can be attributed to an increase in oxygen vacancy ($V_O^{\bullet\bullet}$), resulting from $Zr^{4+}/Sr^{2+}/Yt^{3+}$ substitution. Equation (10)) represent the Yt^{3+} substitution in Ce^{4+} site, generating $V_O^{\bullet\bullet}$. Generated oxygen vacancy can help promote the conversion of CO_2 to CO and creates holes ($h^{\bullet}$), giving in equation (11) and equation (12).

$$2Ce_{Ce}^{X} + Y_2O_3 + O_O^{X} \rightarrow 2Y'_{Ce} + V_O^{\bullet\bullet} + 2CeO_2 \quad (10)$$

$$CO_2 + V_O^{\bullet\bullet} \rightarrow O_O + 2h^{\bullet} + CO \quad (11)$$

$$H_2O + V_O^{\bullet\bullet} \rightarrow O_O + 2h^{\bullet} + H_2 \quad (12)$$

Although BCZ presented low conductivity, the material showed relatively high catalytic activity toward the RWGS reaction. Catalytic surface acidity was also reported to increase with Zr content in other work [33]. The correlation between catalytic surface acidity and Zr content in the electrolyte sample has also become of interest.

1.1.3.4 Research platform 1.1 – Chemical stability

Chemical stability of the electrolyte samples (BC, BSC, BSCY and BCZ) was investigated when exposing to a CO_2-containing gas mixture (10%CO_2, 30%H_2 and 60%N_2, 300 ml min-1 total flow rate) at 600°C for 5 h. Figure 5 presents the XRD patterns of all samples after the test. Impurity peaks (CeO^2) was detected in the BSC and the BSCY samples while both CeO_2 and BaO were detected in the BC sample. The impurity

phase was not observed in the BCZ sample. Although the products from BaCeO3 perovskite reacting with CO2 can be both $BaCO_3$ and CeO_2 [34], $BaCO_3$ was not detected in this study. Barium is easily removed from barium-based electrolyte when reacting with CO_2; leading to BaO formation [35]. The BaO can further react with CO_2 to form $BaCO_3$ [35]. Goldschmidt's tolerance factor is generally used as a criterion for perovskite structure formation. Chemical stability of the barium zirconate-based materials was reported to increase with tolerance factor [13, 17] and the factor was calculated and presented in Table 1. The BCZ exhibited the highest tolerance factor (0.880), follow by BC, BSC, and BSCY, respectively.

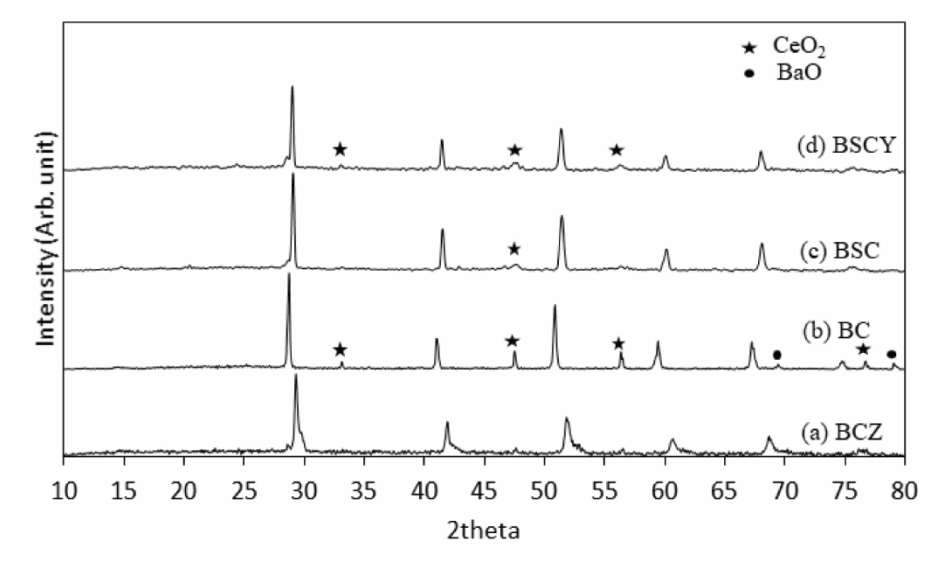

Figure 5 The XRD patterns of the samples after being exposed to CO_2-containing environment

1.1.4 Research platform 1.1 – Conclusion

The BC, BSC, BSCY, and BCZ were successfully synthesized using solid state reaction method with different calcination conditions. The effect of doping Zr^{4+}, Sr^{3+}, and Y^{3+} in barium cerate structure was investigated in term of electrochemical performance and catalytic activity. Activation energy of conduction of barium cerate decreased when doping with Zr^{4+} and Y^{3+}. The BSCY exhibited the lowest activation energy of conduction at 64.69 kJ mol^{-1}. Although the BCZ sample presented relatively low conductivity with high activation energy of conduction (108.12 kJ mol^{-1}), the sample offered high catalytic activity toward the RWGS reaction in terms of CO2 conversion and CO yield. Moreover, the BCZ was rather stable after exposed to CO_2-containing gas mixture at 600^{o}C for 5 h. There was no impurity phase detected in the BCZ sample, unlike the BC, BSC and BSCY samples which showed impurity phases after the exposure. Additional Cu in the form of Cu/electrolyte composite significantly improved catalytic activity toward the RWGS reaction. This implied that the use of cermet-type electrode could be preferable in an CO_2/H_2O-fed electrolyser.

1.1.5 Research platform 1.1 – References

[1] N. Kumar, J.J. Spivey, Direct Conversion of Syngas to Chemicals Using Heterogeneous Catalysts, Encyclopedia of Sustainable Technologies (2017) 605-610.

[2] C. Forman, M. Gootz, C. Wolfersdorf, B. Meyer, Coupling power generation with syngas-based chemical synthesis, Applied Energy 198 (2017) 180-190.

[3] M. Zhao, Y. Cui, J.Sun, Q. Zhang. Modified iron catalyst for direct synthesis of light olefin from syngas, Catalysis Today (2018) In Press.

[4] Y.Ma, Q. Ge, W. Li, H. Xu, Study on the sulfur tolerance of catalysts for syngas to methanol, Catalysis Communications 10 (2008) 6-10.

[5] T-W. Kim, F. Kleitz, J-W. Jun, H-J. Chae, C-U. Kim, Catalytic conversion of syngas to higher alcohols over mesoporous perovskite catalysts, Journal of Industrial and Engineering Chemistry, 51 (2017) 196-205.

[6] S. Akoshima, M. Oishi, K.Yashiro, K. Sato, J. Mizusaki, Reaction kinetics on platinum electrode / yttrium-doped barium cerate interface under H_2–H_2O atmosphere, Solid State Ionics 181 (2010) 240-248.

[7] T. Pua, W. Tana, H. Shia, Y. Naa, J. Luc, B. Zhub, Steam/CO_2 electrolysis in symmetric solid oxide electrolysis cell with barium cerate-carbonate composite electrolyte, Electrochimica Acta 190 (2016) 193-198.

[8] S.K. Jaiswal, S.M. Choi, K.J. Yoon, J.-W. Son, B.-K. Kim, H.-W. Lee, J.-H. Lee, Effect of Ba-deficiency on the phase and structural stability of (BaSr)(CeZr)O_3-based proton conducting oxides, International Journal of Hydrogen Energy 40 (2015) 11022-11031.

[9] X. Chi, Z. Wen, J. Zhang, Y. Liu., Enhanced conductivity of lanthanum niobate proton conductor by A and B-site co-doping: synthesis, phase, microstructure and transport properties, Solid State Ionics 268 (2014) 326-329.

[10] S. Hossain, A.M. Abdalla, S.N.B. Jamain, J.H. Zainia, A.K. Azad, A review on proton conducting electrolytes for clean energy and intermediate temperature-solid oxide fuel cells, Renewable and Sustainable Energy Reviews 79 (2017) 750-764.

[11] M. Stange, E. Stefan, C. Denonville, Y. Larring, P.M. Rorvik, R. Haugsrud, Development of novel metal-supported proton ceramic electrolyser cell with thin film BZY15-Ni electrode and BZY15 electrolyte, International Journal of Hydrogen Energy 42 (2017) 13454-13462.

[12] Y. Wanga, T. Su, W. Liu, Q. Chang, G. Qiao, Effect of indium content on the properties of $BaSn_{0.5}Y_{0.5-x}InxO_{2.75}$ proton conductor, Ceramics International 41 (2015) 6863-6863.

[13] E. Fabbri, A. D'Epifanio, E.D. Bartolomeo, S. Licoccia, E. Traversa, Tailoring the chemical stability of $Ba(Ce_{0.8-x}Zr_x)Y0.2O_{3-\delta}$ protonic conductors for intermediate temperature solid oxide fuel cells (IT-SOFCs), Solid State Ionics 179 (2008) 558-564.

[14] Y. Guo, Y. Lin, R. Ran, Z. Shao, Zirconium doping effect on the performance of proton-conducting $BaZryCe_{0.8-y}Y_{0.2}O_{3-\delta}$ ($0.0 \leq y \leq 0.8$) for fuel cell applications, Journal of Power Sources. 193 (2009) 400-407.

[15] K. Singh, R. Kannan, V. Thangadurai, Synthesis and characterisation of ceramic proton conducting perovskite-type multi-element-doped $Ba_{0.5}Sr_{0.5}Ce_{1-x-y-z}Zr_xGd_yY_zO_{3-\delta}$ ($0 < x < 0.5$; $y = 0, 0.1, 0.15$; $z = 0.1, 0.2$), International Journal of Hydrogen Energy 41 (2016) 13227-13237.

[16] J. Basu, A. Suresh, B.A. Wilhite, C.B. Carter, Microstructural evolution of cobalt-doped barium cerate–zirconate at elevated temperatures under moist reducing conditions, Journal of the European Ceramic Society 131 (2011) 1421-1429.

[17] P. Sawant, S. Varma, B.N. Wani, S.R. Bharadwaj, Synthesis, stability and conductivity of $BaCe_{0.8-x}Zr_xY_{0.2}O_{3-\delta}$ as electrolyte for proton conducting SOFC, International Journal of Hydrogen Energy 37 (2012) 3848-3856.

[18] S. Wanga, F. Zhaoa, L. Zhanga, K. Brinkmanb, F. Chena, Stability and electrical property of $Ba_{1-x}Sr_xCe_{0.8}Y_{0.2}O_{3-\delta}$ high temperature proton conductor, Journal of Alloys and Compounds 506 (2010) 263-267.

[19] S. Hossain, A.M. Abdalla, S.N.B. Jamain, J.H. Zaini, A.K. Azad, A review on proton conducting electrolytes for clean energy and intermediate temperature-solid oxide fuel cells, Renewable and Sustainable Energy Reviews 79 (2017) 750-764.

[20] S. Ricotea, N. Bonanosb, M.C.M.d. Lucasa, G. Cabochea, Structural and conductivity study of the proton conductor $BaCe_{(0.9-x)}Zr_xY_{0.1}O_{(3-\delta)}$ at intermediate temperatures, Journal of Power Sources 193 (2009) 189-193.

[21] Z. Shi, W. Sun, W. Liu, Synthesis and characterization of $BaZr_{0.3}Ce_{0.5}Y_{0.2-x}Yb_xO_{3-\delta}$ proton conductor for solid oxide fuel cells, Journal of Power Sources 245 (2014) 953-957.

[22] P.S. Mahadika, D. Jaina, A.N. Shirsata, N. Manoja, S. Varmaa, B.N. Wania, S.R. Bharadwaja, Synthesis, stability and conductivity of $SrCe_{0.8-x}Zr_xY_{0.2}O_{3-\delta}$ as electrolyte for proton conducting SOFC, Electrochimica Acta 219 (2016) 614-622.

[23] G. Wu, K. Xie, Y. Wu, W. Yao, J. Zhou, Electrochemical conversion of H_2O/CO_2 to fuel in a proton-conducting solid oxide electrolyser, Journal of Power Sources 232 (2013) 187-192.

[24] E. Ruiz-Trejo, J.T.S. Irvine, Electrolysis of CO_2 in a proton conducting membrane, Solid State Ionics 252 (2013) 157-164.

[25] M.P. Carpanese, A. Barbucci, G. Canu, M. Viviani, $BaCe_{0.85}Y_{0.15}O_{2.925}$ dense layer by wet powder spraying as electrolyte for SOFC/SOEC applications, Solid State Ionics 269 (2015) 80-85.

[26] P.A. Stuarta, T. Unnob, J.A. Kilnera, S.J. Skinnera, Solid oxide proton conducting steam electrolysers, Solid State Ionics 179 (2008) 1120-1124.

[27] S. Liu, X. Tan, K. Li, R. Hughes, Synthesis of strontium cerates-based perovskite ceramics via water-soluble complex precursor routes, Ceramics International 28 (2002) 327–335.

[28] P. Pasierb, M. Wierzbicka, S. Komornicki, M. Rekas, Structural, electrical and transport properties of yttrium-doped proton-conducting strontium cerates, Journal of Power Sources 173 (2007) 681–687.

[29] Y.H. Yun, S.M. Nam, Powder synthesis and aerosol deposition of the $BaCe_{0.9}Y_{0.1}O_{2.95}$ and $SrCe_{0.9}Y_{0.1}O_{2.95}$ phases for gas separation membrane application, Ceramics International 37 (2011) 2907–2912.

[30] S. Likhittaphon, T. Pukkrueapun, P. Seeharaj, U.W. Hartley, N. Laosiripojana, P. Kim-Lohsoontorn, Effect of sintering additives on barium cerate based solid oxide electrolysis cell for syngas production from carbon dioxide and steam, Fuel Processing Technology 173 (2018) 119-125.

[31] Y-P. Fu, C-S. Weng, Effect of rare-earth ions doped in $BaCeO_3$ on chemical stability, mechanical properties, and conductivity properties, Ceramics International 40 (2014) 10793-10802.

[32] C. Zhang, H. Zhao. Structural characteristics, sinterability and electrical conductivity of Ba-site non-stoichiometric $Ba_xCe_{0.5}Zr_{0.4}Y_{0.1}O_{3-\delta}$, Materials Research Bulletin 45 (2010) 1659-1663.

[33] C.J. Yoo, D.W. Lee, M.S. Kim, D.J. Moon, K.Y. Lee. The synthesis of methanol from $CO/CO_2/H_2$ gas over $Cu/Ce_{1-x}Zr_xO_2$ catalysts. Journal of Molecular Catalysis A: Chemical 378 (2010) 255-262.

[34] J. LÜ, L. Wang, L. Fan Y. Li, L. Dai, H. Guo. Chemical stability of doped $BaCeO_3$-$BaZrO_3$ solid solutions in different atmospheres. Journal of Rare Earths 26 (2008) 505-510.

[35] R. Gawel, K. Przybylski, M. Vivani, Chemical stability and electrical properties of $BaCe_{0.85}Y_{0.15}O_{3-\delta}$–$Ce_{0.85}Y_{0.15}O_{2-\delta}$ composite bulk samples for use as central membrane materials in dual PCFC–SOFC fuel cells. Materials Chemistry and Physics 147 (2014) 804-814.

Research platform 1

Hydrogen and syngas production from steam and carbon dioxide through solid oxide electrolysis cell (SOEC)

1.2 Effect of sintering additives on barium cerate based solid oxide electrolysis cell for syngas production from carbon dioxide and steam

1.2.1 Research platform 1.2 – Introduction

Solid oxide electrolysis cells (SOECs) are considered as promising system for H_2 and syngas production from steam and carbon dioxide through steam electrolysis application coupling reverse water gas shift reaction, as shown in equation (1)-(4).

Steam electrolysis: $H_2O \rightarrow H_2 + 0.5O_2$ (1)

Anode: $H_2O \rightarrow 2H^+ + 2e^- + 0.5O_2$ (2)

Cathode: $2H^+ + 2e^- \rightarrow 0.5H_2$ (3)

Reverse water gas shift: $H_2 + CO_2 \leftrightarrow CO + H_2O$ (4)

Conventional SOECs consist of oxide ion (O^{2-}) conducting electrolyte such as yttria stabilised zirconia (YSZ) or doped ceria [1-6]. However, proton (H^+) conducting electrolyte has received considerable attention for an application in SOEC [7, 8]. Due to

its much smaller ionic radius, proton mobility is theoretically faster than oxygen-ion [7]. Among the ABO_3 perovskite-type proton-conductor, $BaCeO_3$ exhibits relatively high conductivity (0.04 S cm^{-1} at 600^oC) [9]. However, barium cerate cannot be easily densified at low temperature. High sintering temperature (1500-1700^oC) is required to obtain a relative density above 90% [10, 11]. This leads to issues relating the cell fabrication process; insufficient density of the cell; and, high sintering temperature. Low cell density leads to poor conductivity and gas leakage while high sintering temperature can cause undesired phases and poor chemical homogeneity. The evaporation of BaO can occur at temperature above 1550^oC [12].

Sinterability of polycrystalline ceramics mainly depends on mass transport diffusion mechanism which can be controlled by temperature, time, the size of starting powder, and the addition of sintering aid [1, 13, 14]. Small amounts of transition metal (e.g. Cu, Ni, Fe, Co) have been reported to enhance sinterability of the materials [15-23]. The gadolinium doped barium cerate co-doped by small amounts of transition metal such as 1 %mol Cu was reported to allow a decrease in both calcination and sintering [20].

Transition metals were found to improve the densification of sample; however, their effect on the total conductivity is contradicted since there is a difference between relative density of the sample with and without the additive [13, 17, 20]. The sample added with sintering additive was reported to exhibit lower bulk conductivity [1]. After sintering, residual of sintering additive can incorporate into grain or segregate at grain boundary,

leading to additional unwanted electronic conductivity in the electrolyte or increasing grain boundary resistance. In case of barium-cerate based electrolyte, it is important to determine a positive effect of dense electrolyte on an increased conductivity, comparing to a negative effect of sintering additive residual remaining in the sample. Although the sintering additives have been reported to influence sintering behavior, microstructure, and electrical properties, most of reports are substantially on the field of solid oxide fuel cells and best to our knowledge there is no report on the effect the sintering additive on CO_2/H_2O electrolysis performance in term of both steam electrolysis and CO production which involves the RWGS reaction. Therefore, the focus of this research is toward the effect of sintering additives on the SOEC densification; on the cell electrochemical performance under steam electrolysis conditions; and, on the RWGS reaction. The RWGS reaction was also studied since syngas can be produced through both steam electrolysis reaction and RWGS reaction in an SOEC system

In this research, 0.5-1.5 wt.% of Co_2O_3, NiO and ZnO were added in BCG perovskite as a sintering additive. The influence of the sintering additive on relative density of the electrolyser, electrochemical performance for steam electrolysis (activation energy of conduction) and catalytic performance for carbon monoxide production (CO_2 conversion and CO yield) were investigated. The perovskite phase was prepared using conventional precipitation comparing to ultrasonic-assisted precipitation method to

determine the effect of ultrasonic irradiation on size of starting powder and relative density of the electrolyser.

1.2.2 Research platform 1.2 – Experiment

1.2.2.1 Research platform 1.2 – Synthesis of barium cerate and characterization

A solution of 1M $Ce(NO_3)_3 \cdot 6H_2O$ and 1 M $Ba(NO_3)_2$ (Sigma-Aldrich, 99.9% purity) was prepared as a precursor. A solution of $Ba(NO_3)_2$ was formed by reacting between $BaCl_2 \cdot 2H_2O$ and HNO_3. A solution of 1 M $(NH_4)_2C_2O_4$ was used as precipitating agent (Sigma-Aldrich, purity >98%). To avoid self-precipitation of the concentrated precipitation agent, the precursor was added drop wise into the agent using a feed rate at 60 ml min^{-1}. The solution was continuously stirred using magnetic stirrer at 120 rpm. The reaction was allowed to proceed for 30 minutes after completing addition of the precursors while temperature was maintained at 80^oC. A solution of 1 M $Gd(NO_3)_3$ was introduced to synthesize Gd doped barium cerate synthesis (BCG). For the ultrasonic-assisted precipitation, irradiation of high-intensity ultrasonic (150 W cm^{-2}) was used instead of magnetic stirrer through a direct immersion of an ultrasonic probe into the precipitating solution (Tihorn, Sonic and Material Inc., USA). After completing the precipitation, the precipitate was centrifuged and separated, and washed with DI water

until the washing was neutral. The precipitated was dried at 110 °C for 24 h, followed by calcination at 1000 °C for 5 h. More detail preparation was presented previously [24].

Sintering additive (NiO, Co_2O_3, and ZnO from Sigma-Aldrich, 99% purity) was added into the BCG powder. After that, the mixture was ball milled for 24 h. Due to solubility limit of the additive in the B-sublattice of barium cerate, 0.5-1.5 wt.% of the additive was used in this study [25, 26].

The crystalline phase of sample was determined using X-ray diffraction (XRD, Bruker D8 Advance, Germany). The Debye-Scherrer equation (5) was used to calculate an average crystallite size (*d*) of the sample.

$$d = \frac{0.9\lambda}{\beta_{FWHM}\mathrm{Cos}(\theta)} \qquad (5)$$

where λ is the wavelength, β_{FWHM} is the full-width for the half-maximum (FWHM) intensity peak, and θ is diffraction angle.

The intensity of XRD major peaks was measured and the purity of perovskite phase was presented in term of %perovskite using the following equation (6):

$$\%\mathrm{Perovskite} = \left(\frac{I_{perovskite}}{I_{perovskite} + I_{CeO_2}} \right) x100 \qquad (6)$$

Microstructural images of the sample were taken using scanning electron microscopy (SEM, JEOL JSM-7610F, Japan). The average grain sizes were calculated by linear intersection method.

1.2.2.2 Research platform 1.2 – Sample preparation

An electrolyte-supported cell was fabricated for electrochemical performance measurement. The BCG powder with and without sintering additive was pressed into a pellet (1 metric ton for 2 minutes). The pellet was then sintered at 1450^{o}C for 10 h to obtain an electrolyte pellet with a thickness of ~1.4 mm and a diameter of ~25.0 mm. Silver conductive paste (Sigma-Aldrich, purity ≥ 75%) was deposited on both sides of the electrolyte pellet followed by firing at 900^{o}C for 2 h, giving an electrode with thickness of ~30 μm and area of 0.785 cm^{2}.

The relative density of prepared pellets was determined using equation (7) with the error in relative density less than 1.5%.

$$\text{Relative density} = \frac{\text{Actual density}}{\text{Theoretical density}} \qquad (7)$$

The actual density in this research is bulk density. Closed and opened pores are included in the measured volume. For theoretical density, the unit cell volume was obtained from XRD analysis which provided lattice parameters of the unit cell and theoretical density was calculated using equation (8)

$$\text{Theoretical density} = \frac{(\text{Molecular weight} \times \text{Number of molecules per unit cell})}{\text{Unit cell volume} \times \text{Avogardo's number}}$$

(8)

For catalytic performance measurement, the electrolyte pellet was crushed and sieved (50–60 meshes) to obtain granular catalyst with an average size of ~200 μm.

1.2.2.4 Research platform 1.2 – Electrochemical performance measurement

A current linear sweep method was used to generate I/V curves. Potential was controlled between open circuit voltage and 1.5 V with a scan rate of 20 mV s^{-1} (Metrohm Autolab, Netherlands). The electrolyte-supported cell was placed in the cell holder and was sealed using high-temperature zirconia and zirconium silicate filled adhesive (Untra-Temp 516, Aramco, USA). Platinum wires were used for electrical connection. The cell holder was then placed in a vertical furnace (Chavachot, Thailand) which controlled the cell temperature (400-800°C). The test system allowed variable gas compositions of steam, H_2, and N_2 to be introduced to the electrode. Therefore, at the cathode, a gas mixture of 20%H_2O, 24%H_2 and 56%N_2 was introduced to the electrode chamber (total flow rate of 100 mL min^{-1}). N_2 with the flow rate of 100 mL min^{-1} was used as a sweep gas for H_2 production at the anode. A humidifier used in this study is a bubble column situated inside a thermocirculator bath, to saturate the gas with water at 70°C. The experimental set up for electrochemical performance measurement can be found in our previous publication [24].

The bulk resistance of the cell was obtained from the slope of I/V curve. The cell conductivity was then calculated (8):

$$\sigma = L/RA \quad (8)$$

where σ is conductivity (S cm^{-1}), L is thickness of the cell (cm), R is cell resistance (Ohm) and A is area of electrode (cm^2). The activation energy of conduction (E_a) was calculated using Arrhenius equation (9):

$$\sigma T = A \cdot \exp[-E_a/RT] \quad (9)$$

where σ is conductivity (S cm^{-1}), E_a is activation energy (J mol^{-1}), R is gas constant (8.314 J K^{-1} mol^{-1}), and T is absolute temperature (K).

1.2.2.5 Research platform 1.2 – Catalytic activity measurement

Reverse water gas shift reaction (RWGS) was performed in a 4 mm inner diameter quartz tube reactor, operated under an atmospheric pressure within a temperature range from 400 to 800 ºC with interval of 50ºC using a heating rate of 10ºC min^{-1}. The gas mixture of 10%CO_2, 10%H_2 and 80%Ar was fed with the flow rate of 100 mL min^{-1} to catalyst bed containing 100 mg of catalyst. The feed and product gas streams were analyzed using a Faraday MID detector (QUADERA) and a Mass spectroscopy with a stainless steel capillary (GSD320 O1, Omnistar gas analysis system, Germany). The gas inlet was maintained for 30 minutes until product lines from online-mass spectrometer were steady to ensure steady state and isothermal condition before collecting data at each temperature. The catalyst was taken up to up to 600 ºC at a rate of 10 ºC min^{-1} and

was reduced in situ for 40 minutes in a flow of a 20% H_2/N_2 mixture (50 mL min^{-1}) prior to the reaction.

The experiment in section 2.3 and 2.4 were replicated three times and the reported results were a mean value of three tests. The uncertainty of the measurement was quantified and the error was 0.7-2.1%.

1.2.3 Research platform 1.2 – Results and discussion

1.2.3.1 Research platform 1.2 – Phase formation of BC and BCG

Barium cerate ($BaCeO_3$, BC) and gadolinium-doped barium cerate ($BaCe_{0.9}Gd_{0.1}O_{2.95}$, BCG) were synthesized using conventional precipitation and ultrasonic assisted precipitation method. The XRD patterns of the samples after calcined at 1000^oC for 5 h are presented in Fig.1. It can be seen that the precipitated products contained a mixed phase of a desired phase (BC or BCG) and undesired phase (CeO_2). The XRD patterns showed $BaCeO_3$ with an orthorhombic structure, corresponding to main peaks at (220), (122), (213), (422), (233), (440) and (613) planes, respectively (JCPDS card no. 22-0074). The XRD patterns also showed CeO_2 with a cubic structure, corresponding to main peaks at (200), (213), (400), (311), (420), and (422) planes, respectively (JCPDS card no. 34-394). The detection of CeO_2 means that all the precursors did not completely react (94-95% perovskite formation). However, barium

carbonate was not detected from the samples. The intensity and the width of XRD peaks can be calculated into the %perovskite and the crystallite size and was reported in section 3.1.1.

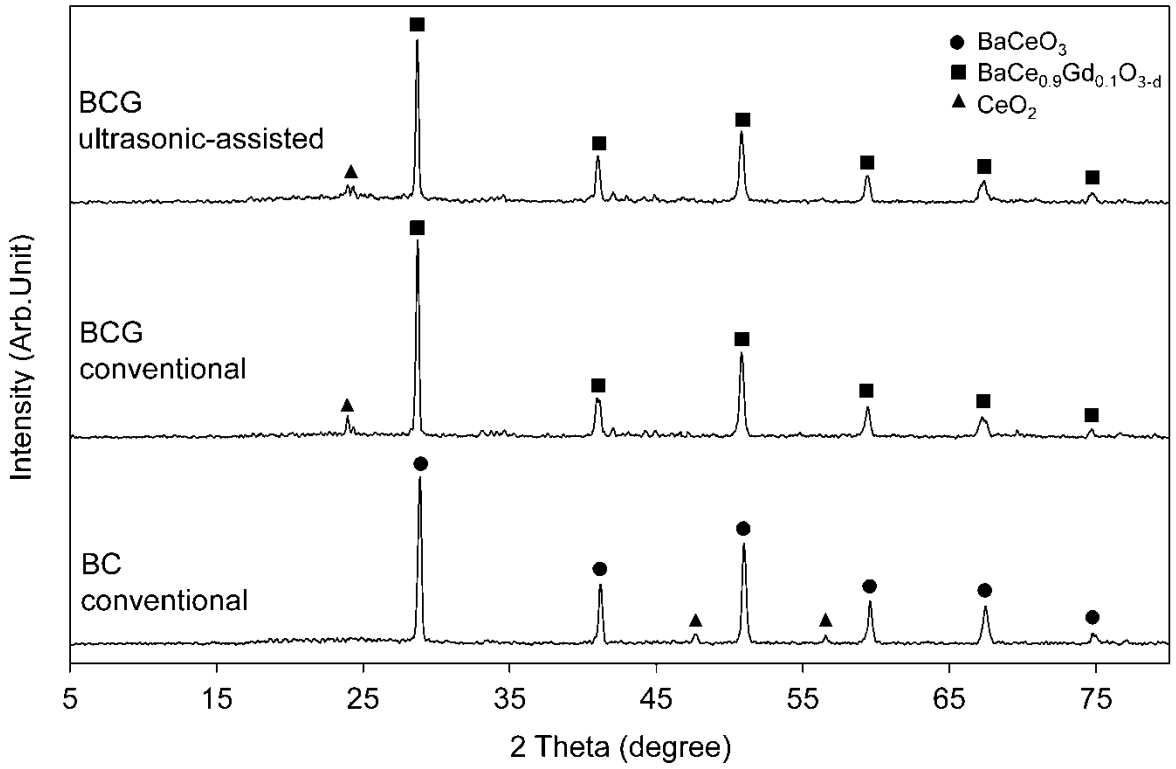

Figure 1 XRD patterns of BC and BCG synthesized by conventional precipitation and ultrasonic-assisted precipitation

1.2.3.2 Research platform 1.2 – %Perovskite, crystallite size, and relative density of BC and BCG

A comparison of BC and BCG in term of %perovskite, crystallite size and relative density are shown in Fig.2. This result demonstrates that doping gadolinium

replacing cerium in the BC structure has no significant impact on %perovskite, crystallite size, and relative density of the sample. The total conductivity of the BCG system was reported to increase with the increase of the gadolinium substitution [20]. The Gd^{3+} was also reported to have higher solubility than others [26, 27]. In term of crystallite size, the Gd^{3+} exhibited slightly higher ionic radius than Ce^{4+}, but the criterion of size matching was acceptable. Doping Gd showed insignificant impact on the cell relative density (62% for BC and 64% for BCG).

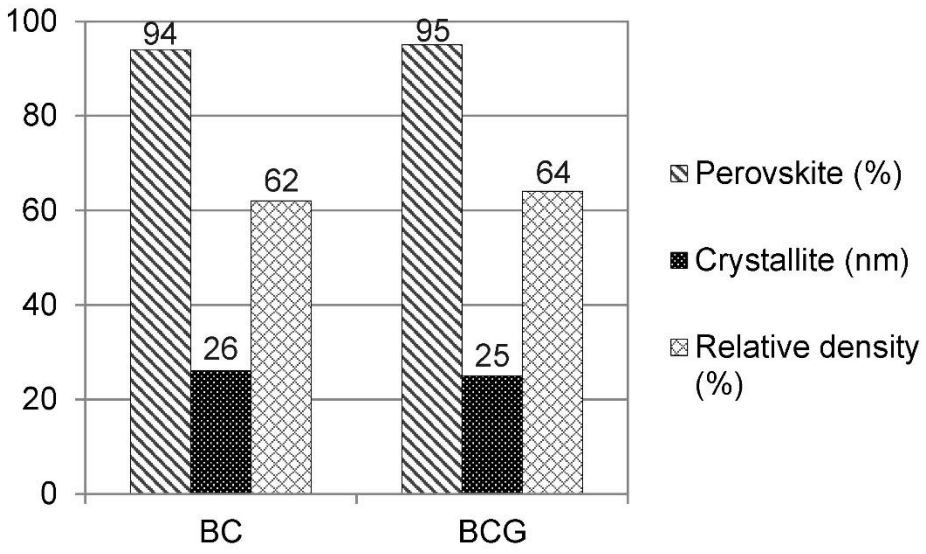

Figure 2 %Perovskite, crystallite size, and relative density of BC and BCG (conventional precipitation)

1.2.3.3 Research platform 1.2 – The effect of synthesis method: ultrasonic assisted precipitation comparing to conventional precipitation

It was known that sinterability and densification of the electrolyte can be improved by controlling nano-particle size and using suitable sintering additives. The effect of synthesis method on %perovskite, crystallite size, and relative density was then investigated and is presented in Fig.3. Ultrasonic-assisted precipitation provided slightly higher %perovskite and smaller crystallite size, likely due to cavitation effect generated from an ultrasonic irradiation. The group of small bubble was formed, gathered and split. This creates the shock wave and increases kinetic and the product formation [24, 28]. The relative density of BCG prepared using ultrasonic-assisted precipitation was 69%, which was slightly higher than BCG prepared using conventional precipitation (64%), relating to smaller crystallite size. This corresponds to the results from the BET measurement. As shown in Table 1, the BET surface area of the precipitated prepared from ultrasonic assisted precipitation was 3.189 m^2/g, while it was 2.691 m^2/g for the precipitated prepared from conventional precipitation. The precipitated from ultrasonic assisted method also had relatively smaller pore size (1.255 x 10^2 Å) and lower pore volume (1.133 x 10^{-3} ml g^{-1}) when compared to the sample from conventional precipitation (pore volume at 1.678 x 10^2 Å and pore size at 9.562 x 10^{-3} ml g^{-1}). Although an alternative preparation method could help increase the cell relative density, the increase was still unacceptable for a dense membrane which generally requires >90% relative density [10,

11]. Therefore, sintering additives were introduced in order to achieve higher relative density of the cell.

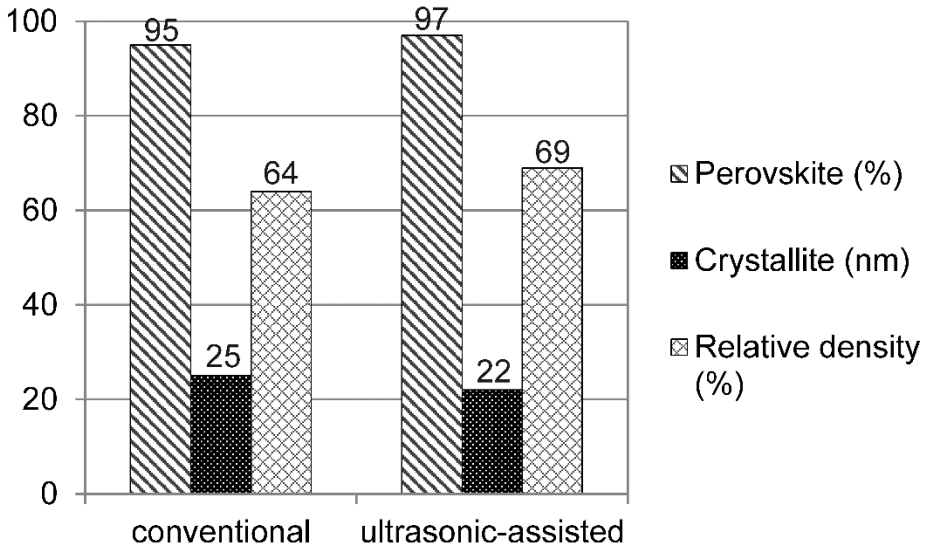

Figure 3 %Perovskite, crystallite size, and relative density of BCG synthesized using conventional precipitation and ultrasonic-assisted precipitation

Table 1 BET surface area, pore size and pore volume of BCG synthesized using ultrasonic assisted precipitation and conventional precipitation

Method	BET surface area (m^2 g^{-1})	Pore size (Å)	Pore volume (ml g^{-1})
conventional precipitation	2.691	1.678×10^2	9.562×10^{-3}
ultrasonic assisted precipitation	3.189	1.255×10^2	1.133×10^{-3}

1.2.3.4 Research platform 1.2 – The The effect of sintering additives: NiO, Co_2O_3, and ZnO

The effect of different types of sintering additives on the cell relative density and microstructure has been investigated. The BCG pellets with and without sintering additives (NiO, Co_2O_3, and ZnO) were sintered at 1450^{o}C for 10 h. The content of the sintering additives was varied from 0.5 to 1.5 wt.%. As shown in Fig. 4, sintering additives had a significant impact on the cell relative density. The BCG with NiO and Co_2O_3 exhibited the same highest relative density at 97% for 1.5 wt.% additives and it was 95% relative density for 1.0 wt.% additives. The BCG with ZnO reached the highest relative density at 88% for 1 wt.% ZnO and the BCG without additive exhibited the cell relative density at only 69%. Babilo et.al [29] reported that Ni, Cu, and Zn were effective to enhance densification. The relative density of these transition metal modified $BaZr_{0.85}Y_{0.15}O_{3-\delta}$ (BYZ) were approximately 86-88% by sintering at 1300°C for 4 h, while the relative density of BYZ without transition metal was only 60%. Guo et.al [30] also reported that introducing of ZnO, the relative density of $BaZr_{0.4}Ce_{0.4}Y_{0.2}O_{3-\delta}$ reached to 90% after sintering at 1150°C for 5 h.

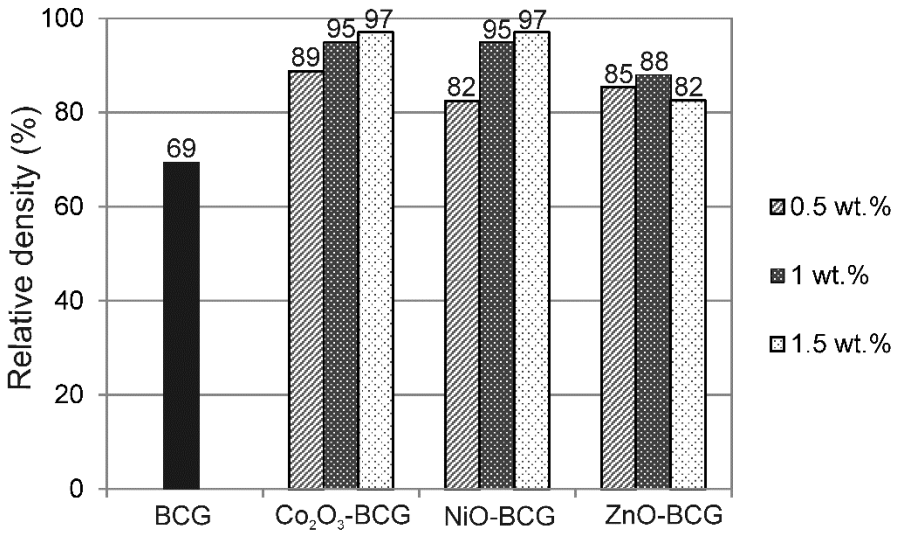

Figure 4 The effect of sintering additives (Co_2O_3, NiO, and ZnO) on relative density of BCG synthesized using ultrasonic-assisted precipitation

The SEM images of bare BCG and the BCG with sintering additives are shown in Fig. 5. In detail, Fig. 5a-5h presents the SEM images of BCG with different sintering additives and different contents. The addition of sintering additive was found to increase both densification and grain growth. In Fig. 5i, it can be seen that there were many open pores along the grain boundaries in the BCG without sintering additive while less open pores and some trapped pores were observed in the BCG with sintering additives. The BCG with the additives also exhibited relatively larger grain size. The addition of transition metals significantly affected microstructure of the sample in this work. Zhang et.al also reported that 1 %wt. ZnO addition enhanced grain growth apparently [19]. However, this contrasts to the work of Amsif et.al [17] which reported that there is no significant impact of sintering aid on the grain size of BCG. The grain size was reported not to depend on the type of sintering additives and the average grain size is similar for an addition of Ni, Zn, Co, and Cu at different contents (0.5-5 mol%) [17]. It should be noted that the temperature used in the work of Amsif et.al [17] was 1200^{o}C for 10 h while it was 1450^{o}C for 10 h in this work and 1300^{o}C for 10 h in the work of Zhang et.al [19]. This implies that

sintering aid may promote densification but not grain growth at low sintering temperature. The average grain size depends on the type and content of sintering additives. As shown in Fig.5, the SEM image of 1.0 wt. % Co_2O_3-BCG was similar to that of 1.5 wt.% Co_2O_3-BCG and the average grain size of Co_2O_3-BCG (13.98 μm) was slightly larger than 1 wt.% NiO-BCG (11.70 μm) and 1 wt.% ZnO-BCG (11.98 μm). The average grain size of bare BCG was only 5.98 μm. As increasing additive content, the grain size increased. The sample with 1.5 wt.% NiO-BCG shows the highest average grain size at 22.78 μm. The data relating to the solubility limit of transition metals in the B-sublattice of barium-cerate-based materials are still uncertain and there are some contradictions in the literature [25]. It was reported that the solubility limit of nickel in B-sublattice of barium cerate, barium zirconate and barium cerate zirconate was very low at 1-2 mol.% while the solubility limit for cobalt was ranging from 0.75-15 mol.% depending on different sintering temperature and preparation method. Tao et.al [31] also reported that if the zinc content was too high, the main perovskite phase decreased, accordingly the formation of Zn-rich perovskite phases. The SEM image of ZnO-BCG was rather different from others. The look-alike impurity phase was observed along with perovskite phase. The densification process of ZnO added barium cerate is reported due to the formation of BaO-ZnO eutectic. In such system, BaO-ZnO or ZnO can co-exist along with the perovskite phase [31].

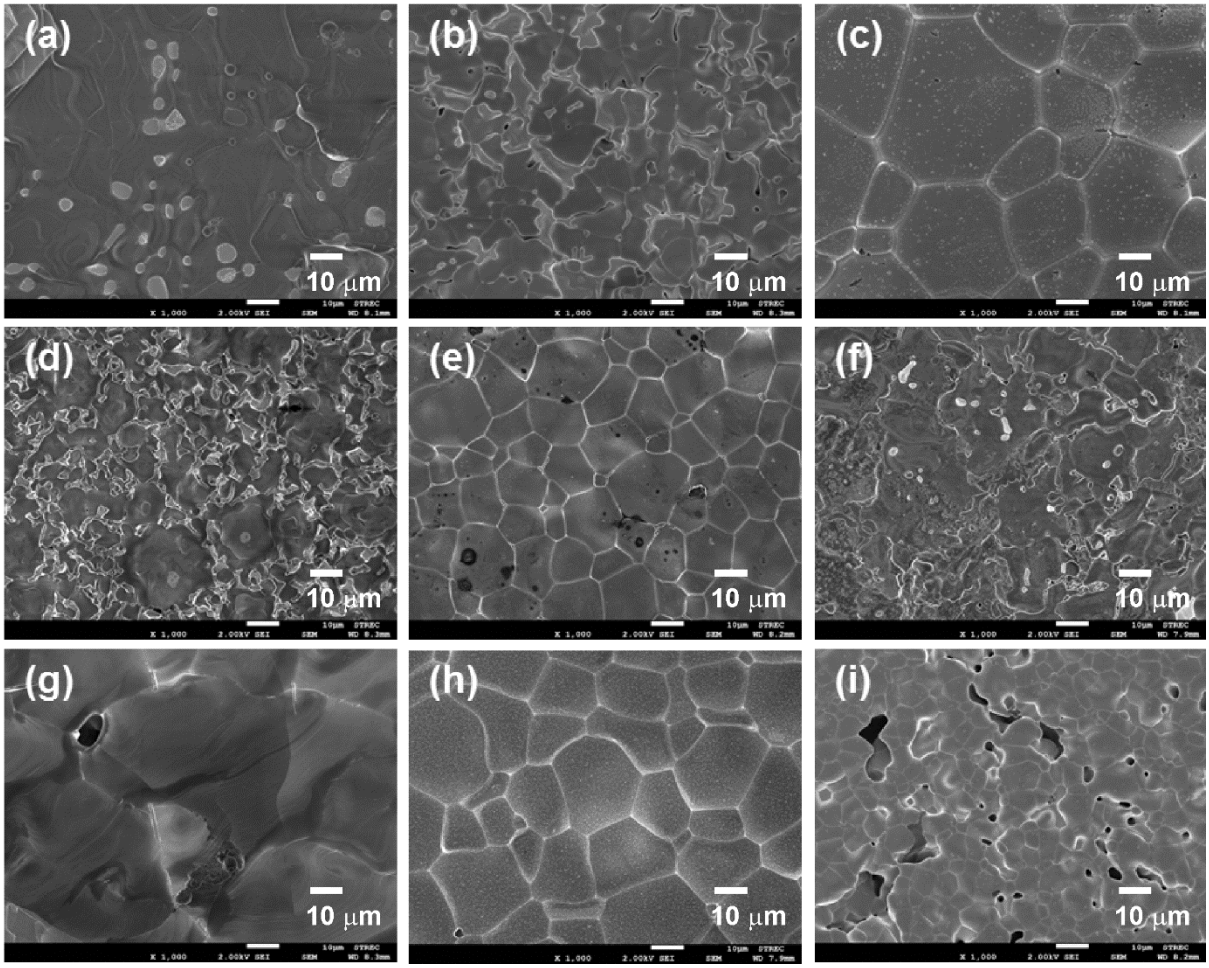

Figure 5 SEM images: (a) 0.5 wt.% NiO-BCG, (b) 1 wt.% NiO-BCG, (c) 1.5 wt.% NiO-BCG, (d) 0.5 wt.% ZnO-BCG, (e) 1 wt.% ZnO-BCG, (f) 1.5 wt.% ZnO-BCG, (g) 0.5 wt.% Co_2O_3-BCG, (h) 1.5 wt.% Co_2O_3-BCG and (i) BCG

1.2.3.5 Research platform 1.2 – The electrochemical performance under steam electrolysis

The sintering additive was known to enhance the relative density through a reduced surface energy and an increasing particle diffusion rate [1, 13, 14]. However, too high content was also reported as negative to the electrochemical performance of the cell due to an introduction of unwanted electronic conductivity. In this work, the BCG with 1

wt.% addition of sintering additives was tested in term of total conductivity. The activation energy of conduction was calculated from I/V curve at temperature from 400-800^{o}C. The uncertainty from the I/V measurement was quantified and it was observed that the error was 2.1%, 0.7%, 2.0% and 1.0% for ZnO-BCG, NiO-BCG, Co_2O_3-BCG and BCG sample, respectively. The sample with sintering additives (ZnO, Co_2O_3, and NiO) exhibited relatively much lower activation energy of conduction leading to higher total conductivity, comparing to BCG without sintering additive as shown in Fig. 6. The activation energy of conduction was 61.80 kJ mol^{-1}, 66.86 kJ mol^{-1}, 70.06 kJ mol^{-1}, and 375.41 kJ mol^{-1} for ZnO-BCG, NiO-BCG, Co_2O_3-BCG, and BCG, respectively. It should be noted that the BCG obtained this study was 97%perovskite which contained CeO_2 as impurity phase and this could lead to reduced proton conductivity of the sample. Among all the additives added, the BCG with ZnO exhibited relatively highest conductivity with the lowest activation energy of conduction. A benefit of ZnO on the electrical properties are due to the fact that ZnO does not lead to an unwanted increase in electronic conductivity in the electrolyte [13, 19, 25, 26, 29-32]. Amsif et.al [17] reported that the grain interior increases slightly after the ZnO addition in $BaCe_{0.9-x}Zr_xY_{0.1}O_{3-\delta}$, whereas the grain boundary decreases due to denser and larger grains [15]. Zhang et.al reported that ZnO addition not only increases the bulk conductivity of $Ba_{1.03}Ce_{0.5}Zr_{0.4}Y_{0.1}O_{3-\delta}$ but also enhances the grain conductivity [19]. However, the sample added with other transition metals was reported to exhibit lower bulk conductivity, especially for samples with cobalt [17]. Babilo et.al [29] reported that the activation energy of $BaZr_{0.85}Y_{0.15}O_{3-\delta}$ with 4 %mol ZnO was 0.47 eV (45.35 kJ/mol) while Presto et.al [33] reported that the activation energy of $BaCe_{0\cdot85}Y_{0.15}O_{2.925}$ with 0.75 wt.% CuO was 0.68 eV (65.61 kJ/mol). The difference in activation energy was likely due to difference in ZnO content, material composition, and gas mixture conditions during measurement. The humidity content used in this study is 20% while it was 3% in the mentioned works.

The color change was observed in the BCG when NiO and Co_2O_3 were introduced. It changed from white to dark green and black upon sintering for NiO and Co_2O_3 addition, respectively. Darker coloring in an oxide can indicate substantial electronic conductivity [29]. Although the transition metals can lead to unwanted increase in electronic conductivity, the higher total conductivity of the samples shown in this study

can be attributed to an increase in density of the samples that leads to denser and larger grain.

It should be noted that in our previous work [24], barium cerate (BC) prepared using ultrasonic-assisted precipitation (150 W cm^{-2}) required a sintering temperature at 1500^{o}C for 10 h to obtain a BC cell having 79% relative density and activation energy of conduction at 75 kJ mol^{-1}. In this work, BCG cell with sintering additives required relatively lower sintering temperature (1450 ^{o}Cfor 10 h) and could reach up to 88-97% relative density and activation energy of conduction ranging from 61.80 to 70.06 kJ mol^{-1}.

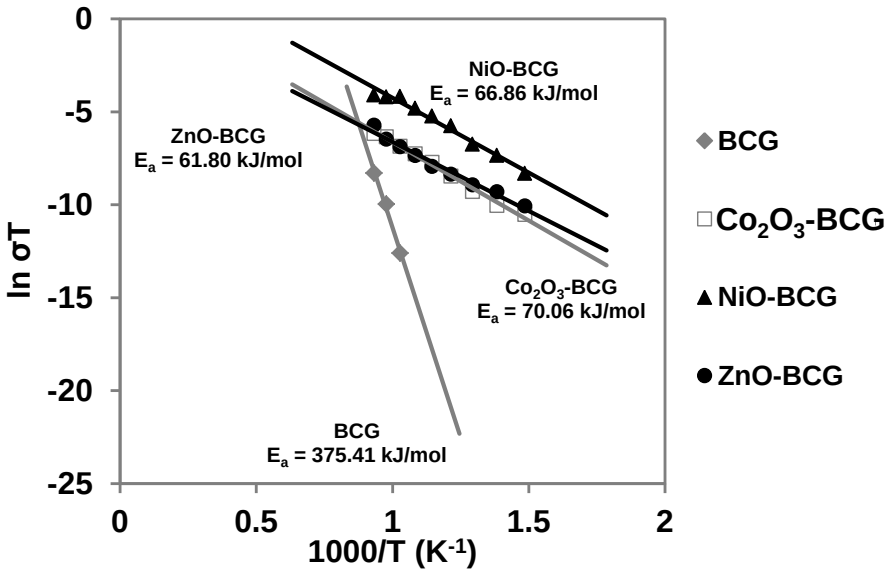

Figure 6 Activation energy of conduction (E_a) for the SOEC fabricated from BCG, BCG-Co_2O_3, BCG-NiO, and BCG-ZnO

1.2.3.6 Research platform 1.2 – The catalytic activity toward RWGS reaction

Since syngas can be produced through steam electrolysis reaction and reverse water gas shift (RWGS) reaction in an SOEC system [34], the effect of sintering additives on the RWGS reaction was also investigated. The bare BCG pellet and the BCG with addition of 1 wt.% sintering additives (NiO, Co_2O_3, and ZnO) were sintered, crashed and

sieved to obtain catalyst granule at 200 μm. Figure 7 and 8 present % conversion of CO_2 and % yield of CO, respectively. It can be seen that the %CO_2 conversion and %CO yield were rather similar for Co_2O_3-BCG, ZnO-BCG and BCG when the temperature was 400-650°C. Above 650°C, the %CO_2 conversion and %CO yield were in the order: Co_2O_3-BCG > BCG > ZnO-BCG. The uncertainly in measure was taken into account. The reported value is a mean value of three replicated measurements and the error in measurement was less than 1.5%.

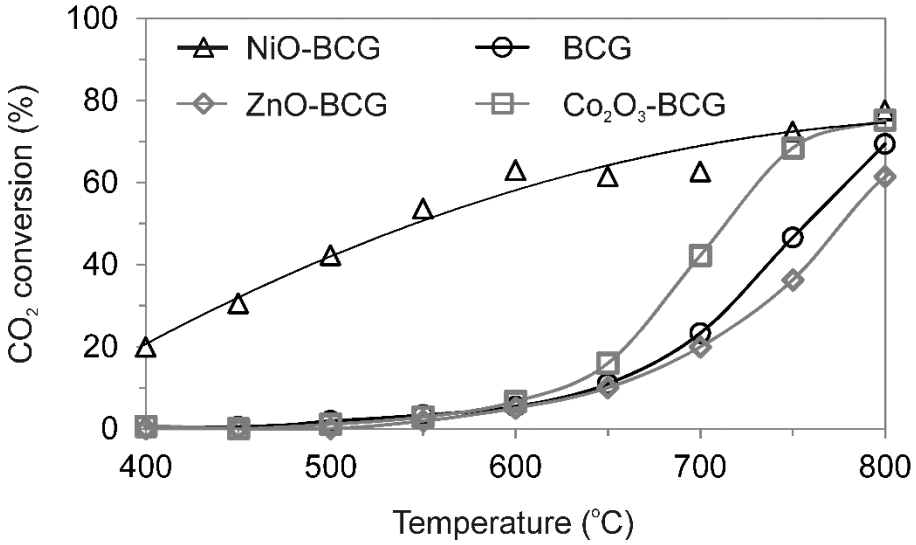

Figure 7 CO_2 conversions toward the reverse water gas shift (RWGS) reaction for BCG, BCG-Co_2O_3, BCG-NiO, and BCG-ZnO catalyst

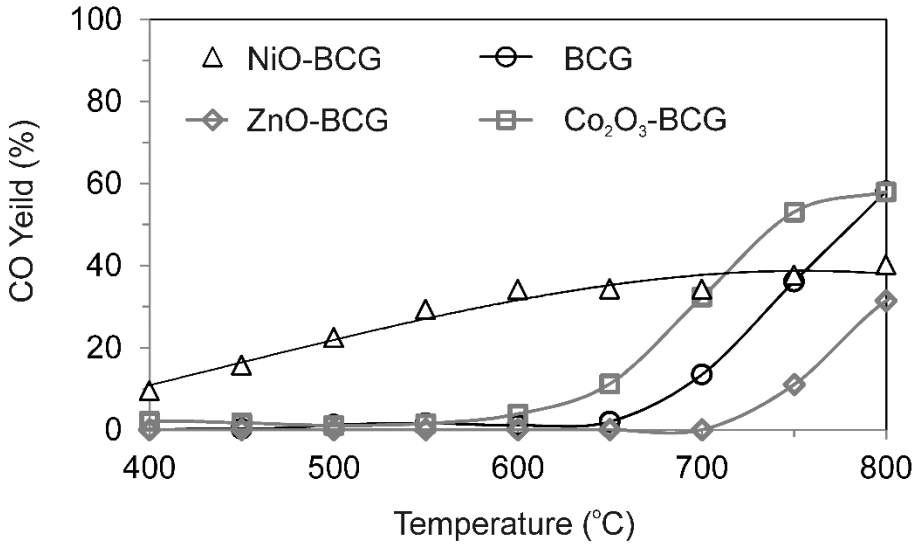

Figure 8 CO yield toward the reverse water gas shift (RWGS) reaction for BCG, BCG-Co_2O_3, BCG-NiO, and BCG-ZnO catalyst

Although ZnO additive could provide relatively highest electrochemical performance, it offered the lowest catalytic performance toward RWGS. The NiO-BCG exhibited significantly higher CO_2 conversion and CO yield than other samples when the operating temperature was below 700°C. Nickel-base catalyst has been studied extensively for RWGS reaction and Ni-CeO_2 catalyst was reported to be active and selective for the RWGS reaction [35, 36]. Above 700°C, CO yield did not increase as CO_2 conversion increased, likely due to carbon deposition on the sample. Figure 9a and 9b presents NiO-BCG before and after the RWGS reaction. Darker color of the catalyst after the test was clearly seen. The temperature program of oxidation (TPO) was also carried out. The used catalyst after the RWGS reaction was exposed to a flow of O_2 while temperature was increased from 400-800°C. Amount of O_2 consumed and CO_2 produced were detected by online-mass spectrometer in which the ion current of main species of mass fragments was followed to indicate carbon deposition. Carbon deposition was calculated and presented in Fig. 9c. Carbon deposition was determined from a differential of carbon molecular in feed and product. As increasing temperature from 400-800°C, the

carbon deposition was increased. At temperature above 700ºC, CO_2 detected from NiO-BCG sample, corresponding to the carbon balance and the result of CO yield.

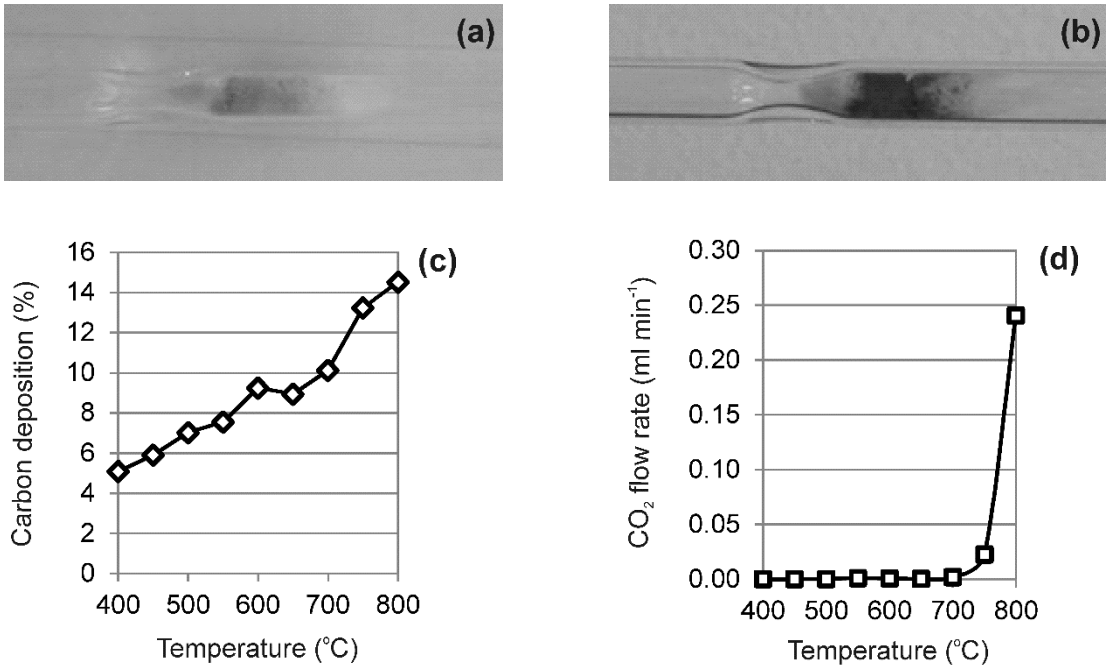

Figure 9 Carbon deposition on NiO-BCG sample: (a) before RWGS test, (b) after RWGS test, (c) calculated carbon balance and (d) the results of temperature program of oxidation (TPO)

1.2.4 Research platform 1.2 – Conclusion

The %perovskite, crystallize size, relative density, electrochemical performance, and catalytic performance of $BaCe_{0.9}Gd_{0.1}O_{2.95}$ (BCG) with sintering additives (NiO, Co_2O_3, and ZnO) were investigated. Although an ultrasonic-assisted precipitation for powder preparation could provide an increase in the cell relative density (69%), comparing to conventional precipitation (64%), the cell relative density was still unacceptable for a dense membrane. Sintering additives significantly affected relative

density, electrochemical performance, and catalytic activity of the cell. Adding NiO and Co_2O_3 as sintering additive, the BCG exhibited the highest cell relative density at 97% for 1.5 wt.% addition and 95% for 1.0 wt.% addition. The ZnO additive provided rather low relatively density (88% for 1.0 wt.% ZnO addition) but the cell with ZnO exhibited the highest electrochemical performance, having the activation energy of conduction at 61.80 $kJmol^{-1}$. In term of catalytic activity, adding ZnO insignificantly affected CO_2 conversion and CO yield while NiO could help increase CO_2 conversion and provided the highest CO yield (32% yield) when operating temperature below 700^oC.

1.2.5 Research platform 1.2 – References

[1] V. Esposito, M. Zunic, E. Traversa, Solid State Ionics, 180 (2009).

[2] M.A. Laguna-Bercero, V.M. Orera, Intermational Journal of Hydrogen Energy, 36 (2011) 13051-13058.

[3] P. Kim-Lohsoontorn, D.J.L. Brett, N. Laosiripojana, Y.-M. Kim, J.-M. Bae, Intermational Journal of Hydrogen Energy, 35 (2010) 3958-3966.

[4] L. Zhang, S. Hu, X. Zhu, W. Yang, Journal of Energy Chemistry, In Press (2017).

[5] J. Yan, L. Shang, Z. Zhao, D. Ou, M. Cheng, Journal of Energy Chemistry, 25 (2016) 840–844.

[6] S. Seetharaman, S.C. Raghu, K.A. Mahabadi, Journal of Energy Chemistry, 25 (2016) 77–84.

[7] Y. Liu, R. Ran, S. Li, Y. Jiao, M.O. Tade, Z. Shao, Journal of Power Sources, 257 (2014) 308-318.

[8] M.A. Laguna-Bercero, Journal of Power Sources, 203 (2012) 4–16.

[9] N.Q. Minh, T. Takahashi, Science and technology of ceramic fuel cells, Elservier Science, Netherlands, 1995.

[10] D. Shima, S.M. Haile, Solid State Ionics, 97 (2007) 443-455.

[11] J. Tong, D. Clark, L. Bernau, A. Subramaniyan, R. O'Hayre, Solid State Ionics, (2010) 1486–1498.

[12] K.H. Ryu, S.M. Haile, Solid State Ionics, 125 (1999) 355–367.

[13] E. Gorbova, V. Maragou, D. Medvedev, A. Demin, P. Tsiakaras, Solid State Ionics 179 (2008) 887-890.

[14] C. Lutgard, D. Jonghe, M.N. Rahaman, Handbook of advanced ceramics, Elsevier Inc, 2003.

[15] M. Amsif, D. Marrero-López, J.C. Ruiz-Morals, S.N. Savvin, P. Núñz, Journal of European Cermics Society, 34 (2014) 1553-1562.

[16] A. Princivalle, G. Martin, C. Viazzi, C. Guizard, Journal of Power Sources, 196 (2011) 9238-9245.

[17] M. Amsif, D. Marrero-López, J.C. Ruiz-Morales, S.N. Savvin, P. Núñz, Journal of Power Sources, 196 (2011) 9154-9163.

[18] C.-L. Tsai, M. Kopczyk, R.J. Smith, V.H. Schmidt, Solid State Ionic, 181 (2010) 1083-1090.

[19] C. Zhang, H. Zhao, N. Xu, X. Li, N. Chen, Internation Journal of Hydrogen Energy, 34 (2009) 2739-2746.

[20] E. Gorbova, V. Maragou, D. Medvedev, A. Demin, P. Tsiakaras, Journal of Power Sources, 181 (2008) 292-296.

[21] S. Ricote, N. Bonanos, Solid State Ionic 181 (2010) 694-700.

[22] M.A. Azimova, S. McIntosh, Solid State Ionics 180 (2009) 160–167.

[23] M. Ananyev, D. Medvedev, A. Gavrilyuk, S. Mitri, A. Demin, V. Malkov, P. Tsiakaras, Electrochimica Acta, 125 (2014) 371–379.

[24] P. Kim-Lohsoontorn, C. Paichitra, S. Vorathamthongdee, P. Seeharaj, Chemical Engineering Journal, 278 (2015) 13-18.

[25] D. Medvedev, A. Murashkina, E. Pikalova, A. Demin, A. Podias, P. Tsiakaras, Progress in Material Science, 60 (2014).

[26] J. Tong, D. Clark, M. Hoban, R. O'Hayre, Solid State Ionics 181 (2010) 496-503.

[27] F. Giannici, A. Longo, K.-D. Kreuer, A. Balerna, A. Martorana, Solid State Ionics 181 (2010) 112-115.

[28] K. Oshima, T. Shinagawa, Y. Nogami, R. Manabe, S. Ogo, Y. Sekine, Catalysis Today 232 (2014) 27-32.

[29] P. Babilo, S.M. Haile, Journal of American Ceramic Society, 88 (2005) 2362–2368.

[30] Y. Guo, R. Ran, Z. Shao., Intermational Journal of Hydrogen Energy, 35 (2010) 5611-5620.

[31] S. Tao, J.T.S. Irvine, Journal of Solid State Chemistry 180 (2007) 3493–3503.

[32] C. Peng, J. Melnik, J.-L. Lou, A.R. Sanger, K.T. Chuang, Solid State Ionic, 18 (2010) 1372-1377.

[33] S. Presto, M. Viviani, Solid State Ionics 295 (2016) 111–116.

[34] Y. Wang, T. Liu, L. Lei, F. Chen, Fuel Processing Technology, 161 (2017) 248–258.

[35] B. Lu, K. Kawamoto, Journal of Environmental Chemical Engineering 3(2013) 300-309.

[36] L. Wang, H. Liu, Y. Liu, Y. Chen, S. Yang., Journal of Rare Earths, 31 (2013) 969-974.

Research platform 2

Methanol production from carbon dioxide and hydrogen through alcohol-assisted method

2.1 Effect of CuO/ZnO catalyst preparation condition on alcohol-assisted methanol synthesis from carbon dioxide and hydrogen

2.1.1 Research platform 2 - Introduction

Fossil fuel is commonly used as a major energy supply, which is also a main source of CO_2 emission [1-5]. Currently, CO_2 emission is 6.2 million tons per year, and tends to increase each year. The increasing CO_2 concentration in atmosphere was predicted to be 44% from 2006 to 2030 [6]. Carbon capture and sequestration (CCS) has been proposed as a strategy to decrease accumulated CO_2 in the atmosphere. However, the technological challenge still remains as it is not possible to evaluate the impact of storing large amount of CO_2 into uncontrolled undergrounds layers. The leakage of the gas back to the surface is still a concern. Therefore, a utilization of CO_2 into valuable chemicals is of great interest [7-10].

Methanol is one of the primary feedstock for many industrial chemical productions, such as formaldehydes, acetic acid, methyl tertiary butyl ether (MTBE) or

dimethyl ether (DME), which are necessary for other industrial sectors such as transportation and construction [11-13]. Currently, methanol consumption is about 65 million tons per year, while 75 percent of the world methanol has been produced from syngas ($CO+H_2$). However, syngas is normally derived from natural gas which is a limited natural resource and the reforming process results in CO_2 emission [14, 15]. In this research, methanol has been synthesized directly from CO_2 and H_2 through a process called alcohol-assisted methanol synthesis.

In general, methanol can be produced from CO or CO_2 with H_2 through equilibrium reactions (Eqs, (1) and (2)), which are based on catalytic hydrogenation [16, 17]. The reactions are naturally highly exothermic; therefore, low temperature is thermodynamically required.

CO-rich methanol synthesis; $CO + 2H_2 \leftrightarrow CH_3OH$ (1)

ΔH_{298}= -90.97 kJ mol^{-1}

CO_2-rich methanol synthesis; $CO_2 + 3H_2 \leftrightarrow CH_3OH + H_2O$ (2)

ΔH_{298}= -49.43 kJ mol^{-1}

However, when using conventional reaction pathways, methanol is well synthesized at rather high temperature and pressure (523-573 K, 5-10 MPa) [18-30]. Therefore, a conflict between highly exothermic reaction and high reaction temperature is a challenge for conventional methanol synthesis process. Alcohol-assisted low

temperature methanol synthesis was firstly proposed by Tsubaki et.al [31]. An addition of alcohol changes the reaction pathway and the process can be carried out at relatively lower operating temperature and pressure (423-443 K and 3-5 MPa) [13, 25, 31, 32]. The reaction pathway consisted of five reaction steps, shown in Eqs. (3-7):

$$CO + H_2O \rightarrow CO_2 + H_2 \quad (3)$$

$$CO_2 + 1/2H_2 + Cu \rightarrow HCOOCu \quad (4)$$

$$HCOOCu + ROH \rightarrow HCOOR + CuOH \quad (5)$$

$$HCOOR + 2H_2 \rightarrow ROH + CH_3OH \quad (6)$$

$$CuOH + 1/2H_2 \rightarrow H_2O + Cu \quad (7)$$

For Eq. (4), formate is well-recognized as an intermediate for the water-gas shift reaction, presented in Eq. (3). In a conventional route, hydrogenation of formate species which is an intermediate for methanol synthesis is available at 523-573 K. In an alcohol-assisted route, the hydrogenation of formate species is decreased to 298-443 K when adding ethanol into the system [25]. In addition, the ethyl formate ($HCOO\text{-}C_2H_5$), the hydrogenation product of formate species from alcohol assisted route, is very easy to be reduced by active hydrogen atoms to form methanol (Eq. (6)). Equation (5) is an esterification reaction which preferably proceeds over an acidic catalyst. Methanol is generated through Eq. (6) which can be operated at 453 K and 3 MPa on modified Cu-

based catalyst [31]. The structure of Cu–Zn–O was reported to be the main active site for the reaction in Eq. (3), while a copper-based site is for the reaction in Eq. (6). Therefore, CuO/ZnO has been considered as an efficient catalyst for methanol synthesis in this reaction. Various catalyst modification was proposed to offer high catalytic activity for methanol synthesis such as the Al, Ce, and Zr modified Cu-ZnO [30] or Pd-Cu alloy catalyst [41]. It should be noted that alcohol (ROH) is not consumed in the net reaction of alcohol assisted method (Eqs. (1)-(7)).

Preparation conditions of CuO/ZnO catalyst have been reported to significantly affect the catalyst properties and their activities [11]. Either dry-chemical technique or wet-chemical technique can be used to prepare the catalyst. For the dry process, a solid state reaction is generally used. It was reported that the calcination conditions such as temperature, time, and gas-containing environment are crucial for a catalyst performance [33, 34]. A solid state reaction can be simplified but high temperature calcination is often required which leads to inhomogeneous product with a large crystallite size. A co-precipitation is one of wet chemical techniques in which reactants are mixed in an atomic-level, resulting in small particle products with narrow size distribution. The parameters for catalyst synthesis conditions such as precipitating pH, temperature, aging time, and Cu to Zn ratio are reviewed for their effects on catalyst properties such as surface area, crystallite size, and surface acidity relating to the catalyst performance during methanol synthesis [25, 31, 32, 35, 36]. Ultrasonic-assisted precipitation is a high performance

method for controlling shape and size distribution of products. The energy from ultrasonic waves leads to acoustic cavitation. The accreted and popping of bubble create a frequency which is a cause of local heating swapping with extreme cooling. This phenomenon generates a homogeneous mixing [37]. In this study, the use of ultrasonic during precipitation exhibited a potential to be applied for CuO/ZnO preparation. The precipitation temperature could be reduced while the catalyst properties were improved.

The challenge of this research has been divided into two parts, which are CuO/ZnO catalyst preparation using ultrasonic-assisted precipitation; and, methanol synthesis using alcohol-assisted method. Effects of catalyst preparation parameters (precipitation temperature, pH, and ultrasonic irradiation) as well as the methanol synthesis conditions (alcohol type) were investigated.

2.1.2 Research platform 2 - Experimental

2.1.2.1 Research platform 2 - Preparation of CuO/ZnO using conventional precipitation

The CuO/ZnO catalysts were synthesized by a conventional precipitation with different precipitation temperatures (298-353 K) and pH values (5-9). Copper nitrate ($Cu(NO_3)_2 \cdot 3H_2O$, Sigma–Aldrich, ≥98%) and Zinc nitrate ($Zn(NO_3)_2 \cdot 6H_2O$, Sigma–Aldrich, ≥99%) were used as metal precursors by fixing the atomic ratio of Cu/Zn at 1/1 while 1 M

sodium carbonate (Na_2CO_3, Sigma–Aldrich, ≥99.5%) was used as a precipitating agent. The precursor was added drop wise to the precipitation agent such that the concentrated agent could be stirred to avoid self-precipitation. The ratio of precipitated product to precipitating agent was 5 g to 600 ml. The precursor feed rate was 0.5 ml min^{-1}. The solution was stirred using magnetic stirrer at 120 rpm in case of conventional precipitation. The reaction was allowed to proceed for 1 h at controlled precipitation temperature (298-353 K) after completing addition of the precursors. During the precipitation process, the temperature was controlled from ambient temperature to 353 K and the pH value was controlled from 5 to 9 with an interval of 1 using a Na_2CO_3. The precipitated product was washed with distilled water to remove sodium ion and then centrifuged. The washing solution was measured using a conductivity meter to check the remaining ion. Consequently, the precipitated samples were dried at 378 K for 24 h and calcined in air at 623 K for 1 h with a heating rate of 10 K min^{-1}.

2.1.2.2 Research platform 2 - Preparation of CuO/ZnO using ultrasonic assisted precipitation

The ultrasonic-assisted precipitation technique was used to synthesize CuO/ZnO comparing to the conventional precipitation. The CuO/ZnO was prepared with the same precursors and process used in the conventional precipitation. An ultrasonic

probe was inserted into the solution instead of using a magnetic bar. The ultrasonic intensity was maintained at 50 W cm^{-2}. The ratio of precipitated product to precipitating agent was maintained as same as that of the conventional precipitation. Precipitation temperature was varied from 298-353 K while pH was maintained constantly at 7. After that, the precipitated sample was washed, centrifuged, dried at 378 K for 24 h, and calcined in air at 623 K for 1 h with a heating rate at 10 K min^{-1}. There are reported that lower calcination temperature is propitious to get a higher Cu dispersion, a smaller Cu crystal size [4, 30].

2.1.2.3 Research platform 2 - Catalyst characterization

Crystallite phases of the catalysts were investigated by x-ray diffraction (XRD, Rigaku, MiniFlex II) using Cu-Kα (λ= 1.541841 Å). The XRD patterns were measured with 2θ from 10 to 80 degrees with a scanning rate of 2 degree min^{-1} at 30 kV and 15 mA. The crystallite size (d) of the catalysts was calculated using Scherrer's equation (8).

$$d = \frac{0.9\lambda}{\beta_{FWHM}Cos(\theta)} \quad (8)$$

where λ is the wavelength, β_{FWHM} is the full-width for the half-maximum (FWHM) intensity peak, and θ is the diffraction angle.

The Brunauer–Emmett–Teller (BET) surface area of catalysts was analyzed using nitrogen adsorbed-desorbed (Autosorb 1-AG, Quantachrome). The scanning electron microscopy – energy dispersive spectroscopy (SEM-EDS) images (Jeol, JSM-6610) were taken to investigate the surface morphology of the catalysts.

The reduction temperature of the catalysts was analyzed using the Temperature Program of Reduction (TPR, Chembet 3000) by placing the catalysts in a flow reactor. After placing the catalysts in a flow reactor, they were heated to 423 K in N_2 atmosphere to dry the sample. The reactor was then taken up to 773 K at a heating rate of 20 K min^{-1} under 80 ml min^{-1} flow of H_2.

The surface acidity of the catalysts was analyzed using ammonia temperature program of desorption (NH_3-TPD, Bel-Cat B) by packing the catalysts in a quartz reactor which is located inside the TPD equipment. Helium gas was introduced at 473 K for 1 h to remove the adsorbed organic impurities on the surface of the catalysts. Subsequently, NH_3 was added at 473 K to be adsorbed on the acid sites of the catalyst. After that, the sample was left at 323 K for 1 h to remove the unabsorbed NH_3. The temperature range of 303–873 K with a heating rate of 10 K min^{-1} was used in all experiments.

2.1.2.4 Research platform 2 - Alcohol-assisted methanol synthesis

In this research, a method called alcohol-assisted methanol synthesis was used. The methanol was synthesized from CO_2 and H_2 as reactants. The experimental set up including schematic drawing and test rig is presented in Fig. 1. The 3 g of catalyst was loaded in a batch reactor. The catalyst was reduced in-situ in the reactor under H_2 gas flow with a flow rate of 30 ml min^{-1} at 573 K for 3 h to convert CuO/ZnO into Cu/ZnO. After that, 50 ml of alcohol (ethanol, propanol and butanol) was introduced, and the reactant gas was fed with CO_2 and H_2 at the molar ratio of 1:3 (CO_2:H_2), controlled using mass flow controllers (GFC17, AALBORG). The reactor was initially pressurized to 3.6 MPa and heated to 423 K. During the heating process, the reactor pressure was increased to 5 MPa at 423 K. Vigorous stirring was applied at 1000 rpm for 24 h. When the reaction was complete, the reactor was left to cool down to room temperature, and the liquid products were collected for methanol analysis.

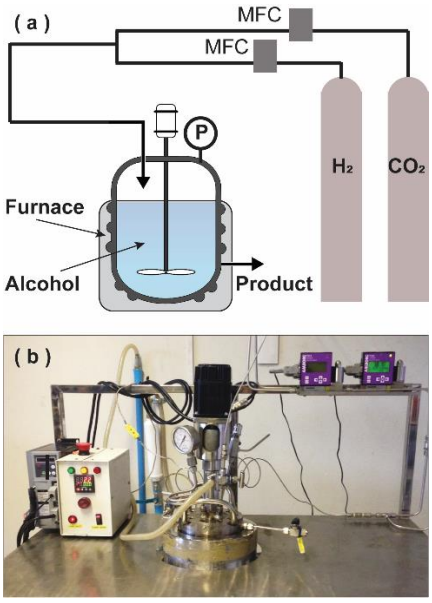

Figure 1 Experimental setup: **(a)** schematic drawing and **(b)** test rig

The products were analyzed using gas chromatography (Clarus680, PerkinElmer) having the COL-VELOCITY column (30 m x 0.32 mm I.D. 0.25 μm film thickness). Finally, the conversion of CO_2, and yield and selectivity of methanol were calculated (Eqs. 9-11).

$$\%CO_2 \text{ conversion} = \frac{\text{Mole of converted } CO_2}{\text{Mole of feeding } CO_2} x100 \quad (9)$$

$$\text{Yeild of methanol} = \frac{\text{Mole of methanol product}}{\text{Mole of feeding } CO_2} x100 \quad (10)$$

$$\text{Selectivity of methanol} = \frac{\text{Mole of methanol product}}{\text{Mole of all products}} x100 \quad (11)$$

2.1.3 Research platform 2 - Results and Discussion

2.1.3.1 Research platform 2 - Effect of precipitation temperature

The CuO/ZnO catalysts were successfully synthesized at different conditions, confirmed by the XRD patterns shown in Fig. 2. The XRD patterns showed CuO and ZnO phases corresponding to main peaks at (111) for CuO ($2\theta=39^o$, ref. JCPDS card no. 45-

0937) and (101) planes for ZnO ($2\theta=36^{o}$, ref. JCPDS card no. 79-0206). The crystallite size of CuO and ZnO were calculated using the Scherrer's equation, as shown in Table 1. Fig. 2(a) shows the XRD patterns of CuO/ZnO synthesized at different temperatures (239-353 K) with constant solution pH of 7. It can be seen that the catalysts precipitated below 333 K exhibited relatively lower crystallite size. The crystallite growth rate is known to linearly increase with increasing temperature, while nucleation rate exponentially decreases [35]. Consequently, as increasing the precipitation temperature, the crystallite size decreased in the early stage. At above 353 K, the crystallite growth rate becomes relatively higher than the nucleation rate, leading to relatively larger crystallite size. The BET surface area of catalysts was determined as presented in Table 1. The catalysts with relatively smaller crystallite size exhibited larger BET surface area, and the largest BET surface area was obtained from the catalyst precipitated at 333 K (80.02 $m^2\ g_{cat}^{-1}$).

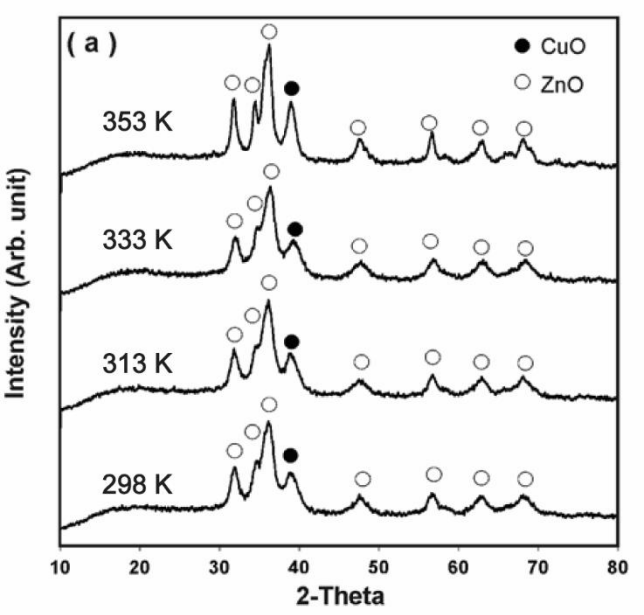

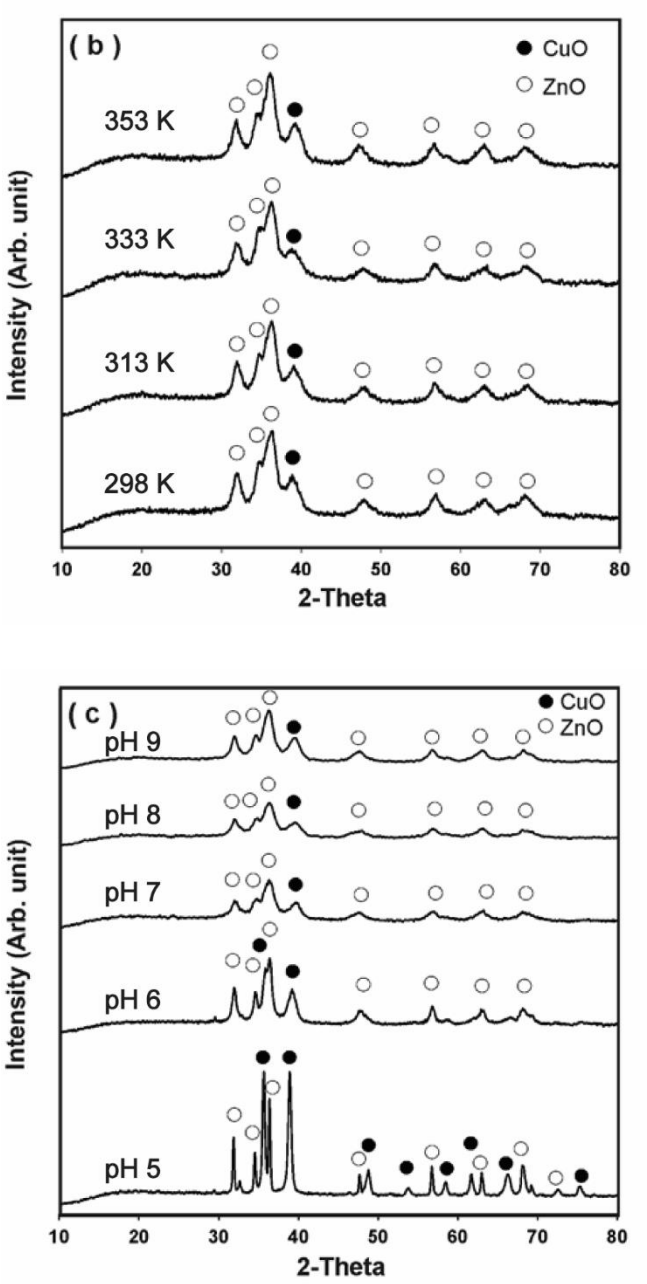

Figure 2 The XRD patterns of CuO/ZnO synthesized at different conditions: **(a)** conventional precipitation at different temperatures (239-353 K); **(b)** ultrasonic-assisted precipitation at different temperatures (239-353 K); and **(c)** conventional precipitation at different pH (5-9)

Table 1 Specific surface area, crystallite size and reducing temperature of the catalysts synthesized using different precipitation temperatures, pH values, and ultrasonic intensity

Catalysts	Specific surface area ($m^2\ g_{cat}^{-1}$)	Crystallite size (nm)		Reducing temperature (K)
		CuO (111)	(ZnO (101)	
CuO/ZnO_298 K_C	67.63	5.83	6.40	359.2
CuO/ZnO_313 K_C	67.83	5.70	6.61	347.4
CuO/ZnO_333 K_C	80.02	5.60	6.56	351.8
CuO/ZnO_353 K_C	41.70	7.24	7.65	404.1
CuO/ZnO_298 K_U	75.00	4.87	6.03	341.8
CuO/ZnO_313 K_U	73.02	4.33	3.57	334.0
CuO/ZnO_333 K_U	102.15	4.02	6.26	335.5
CuO/ZnO_353 K_U	74.23	4.49	4.82	383.0
CuO/ZnO_pH 5_C	8.00	23.13	19.64	514.1
CuO/ZnO_pH 6_C	30.00	8.01	7.45	429.5
CuO/ZnO_pH 7_C	80.02	6.63	7.01	352.2
CuO/ZnO_pH 8_C	90.67	5.56	6.08	327.4
CuO/ZnO_pH 9_C	52.73	6.32	6.66	359.9

Catalyst reducing temperature was investigated using the TPR, as presented in Table 1. The catalysts precipitated at 313 and 333 K exhibited relatively lower reducing temperature than catalysts precipitated at 298 K and 353 K. The low reducing temperature can be attributed to the reduction of highly dispersed CuO/ZnO catalyst [4]. In addition, the lower reducing temperature may provide slower grain growth rate, leading to a smaller crystallite size of catalyst.

Among the reaction pathways of the alcohol-assisted methanol synthesis, the esterification reaction in Eq. (3) was reported as the rate determining step, and this reaction can be facilitated on an acid-site of catalyst [14]. In this study, the surface acidity of the catalyst was determined using NH_3-TPD. Peak deconvolution of NH_3-TPD reveals

that all Cu/ZnO catalysts in this study exhibited three types of acid sites, and the corresponding results are summarized in Table 2. The weak, the medium, and the strong acid sites corresponds to the NH_3-TPD peaks observed in the temperature range of 333–443 K, 463–583 K, and 583–683 K, respectively. It can be seen in Table 2 that the catalyst precipitated at 298 K obtained the highest total surface acidity (0.37 mmol NH_3 g_{cat}^{-1}); however, the strong acid site was not found. In this study, the relation between acidity strength distribution and precipitation temperature is still unclear. However, it was observed that not only a large amount of total acidity and strong acid sites are required but the surface acidity distribution is also important factor to determine the catalytic activity in this reaction.

Table 2 Acid properties of the surface of the catalysts synthesized at different precipitation temperatures, precipitation solution pH values, and ultrasonic intensity

Catalysts	Acidity (mmol NH_3 g_{cat}^{-1})			
	Weak acid site	Medium acid site	Strong acid site	Total acidity
CuO/ZnO_298 K_C	0.095	0.275	-	0.370
CuO/ZnO_313 K_C	0.037	0.053	0.077	0.166
CuO/ZnO_333 K_C	0.040	0.122	0.029	0.191
CuO/ZnO_353 K_C	0.019	0.022	0.072	0.113
CuO/ZnO_298 K_U	0.101	0.301	0.005	0.407
CuO/ZnO_313 K_U	0.095	0.183	0.102	0.380
CuO/ZnO_333 K_U	0.075	0.057	0.331	0.463
CuO/ZnO_353 K_U	0.103	0.090	0.155	0.348
CuO/ZnO_pH 5	0.006	0.015	0.050	0.071
CuO/ZnO_pH 6	0.025	0.021	0.081	0.126
CuO/ZnO_pH 7	0.035	0.024	0.157	0.217
CuO/ZnO_pH 8	0.036	0.022	0.176	0.234
CuO/ZnO_pH 9	0.027	0.039	0.090	0.156

The SEM images also revealed that the catalyst precipitated at 298 K obtained different morphology from others (239-353 K). As presented in Figs. 3 (a)-(d), when SEM images were magnified, the precipitated product was seen to exhibit rod-like morphology with different length of the rods (< 1 μm) while the catalyst was seen to agglomerate as spherical shape in a large scale with a dimeter < 7 μm) (Figs. 3(e) and (f)). The precipitated sample at 298 K contained rather large rods mixed with plate-like structures. It is known that zincian-malachite [$(Cu,Zn)_2(OH)_2CO_3$] exhibits rod-like morphology [38] which is normally a preferred phase [39]. Aurichalcite [$(Cu,Zn)_5(OH)_6(CO_3)_2$ generally exhibits plate-like morphology and a large plate-like morphology was reported to develop in zinc-rich samples [38]. Various precipitated CuO/ZnO morphology was reported depending on Cu/Zn ratio of the precipitate [38, 40, 41], aging time [8], and pH value [32].

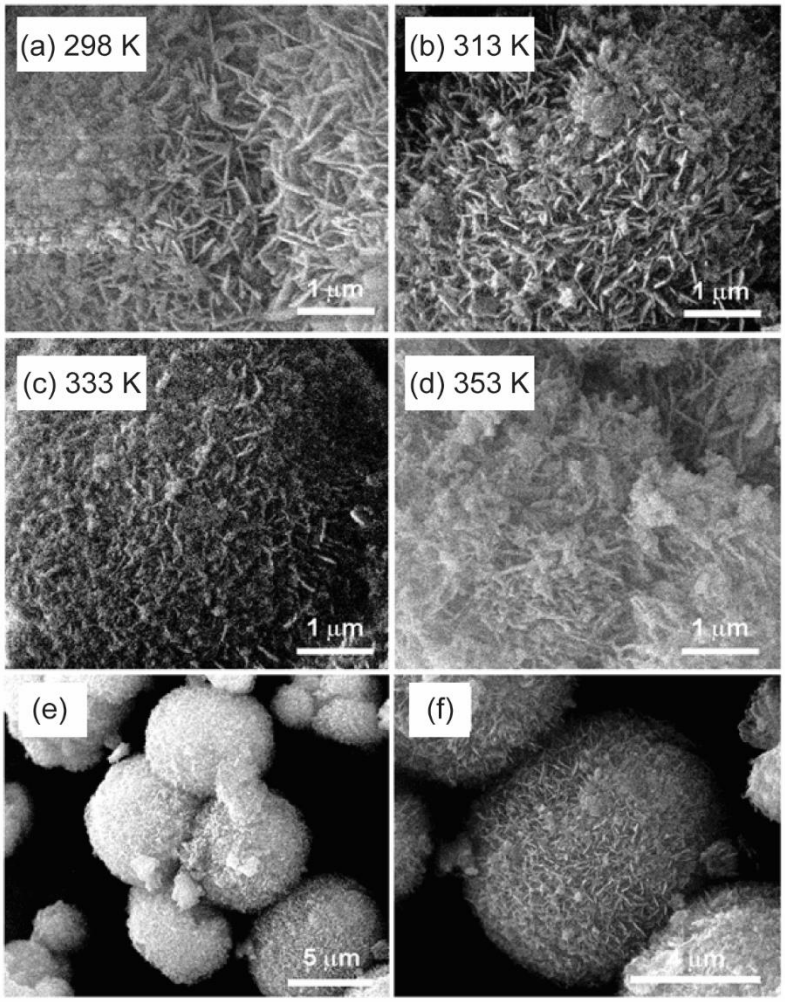

Figure 3 SEM images of the catalysts synthesized at **(a)** 298 K, **(b)** 313 K, **(c)** 333 K, **(d)** 353 K, **(e)** and **(f)** magnified scales of Figure 3(c)

However, in this study precipitation temperature also affected the precipitate morphology. Moreover, it should be noted that the color change of mother liquor from blue to green was observed in all samples during precipitation, except the precipitation at 298 K which remained as blue solution. After 1 h of aging time, the color change was completed. It was reported that the color change of mother liquor after a certain aging

time indicates a formation of hydroxylcarbonate crystalline such as malachite [$Cu_2CO_3(OH)_2$], zincian-malachite and aurichalcite [35, 42, 43] which are precursors of required catalyst after calcination.

The catalytic activity toward methanol synthesis (in terms of methanol yield and selectivity as well as CO_2 conversion) was determined. As presented in Fig. 4, the precipitation temperature during catalyst synthesis significantly affected methanol yield and CO_2 conversion. Methanol yield increased with increasing precipitation temperature. The maximum yield at 31% was obtained from the CuO/ZnO catalyst prepared at 333 K, consistent with relatively small CuO crystallite size (5.83 nm), large BET surface area (80.02 $m^2\ g_{cat}^{-1}$), low reducing temperature (624.8 K) and high surface acidity (0.191 mmol $NH_3\ g_{cat}^{-1}$). At 353 K precipitation, methanol selectivity increased but yield decreased. This corresponds to the work of Farahani et al. [35] which reported that the catalysts aging at 333 K provided the smallest CuO crystallite size, the highest Cu surface area and STY (space time yield) of methanol.

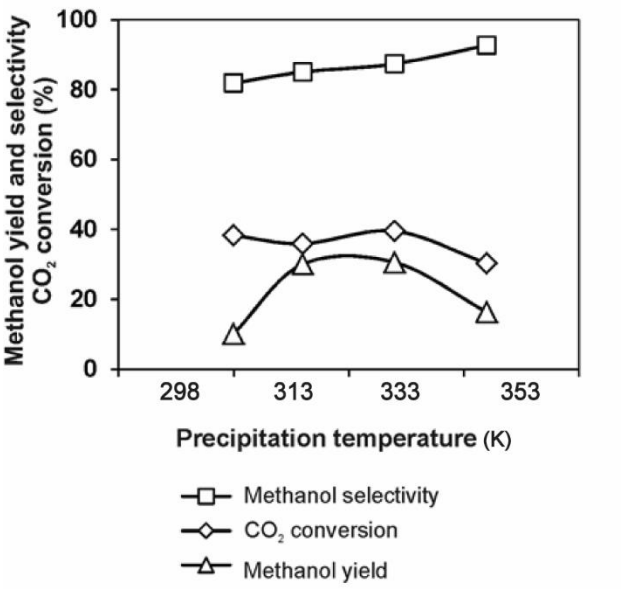

Figure 4 Yield and selectivity of methanol and CO_2 conversion using the catalysts synthesized through conventional precipitation at different temperatures (298, 313, 333, and 353 K)

2.1.3.2 Research platform 2 - Effect of ultrasonic irradiation during precipitation

The ultrasonic-assisted precipitation technique was used to synthesize CuO/ZnO comparing to the conventional precipitation. Precipitation temperature was varied from 239-353 K while pH was maintained constantly at 7 and the ultrasonic intensity of 50 W cm^{-2} was applied during precipitation. Phases of the catalysts were investigated using XRD investigation, as shown in Fig. 2(b). The XRD patterns of the catalysts exhibited CuO/ZnO crystallized phases, and the catalyst crystallite sizes were calculated.

Table 1 presents that ultrasonic-assisted precipitation helped increase the BET surface area of catalyst. Moreover, the requirement for precipitation time decreased from 1 h to 0.5 h. The color change of mother liquor was observed after 0.5 h of aging time when ultrasonic was used, indicating that the ultrasonic wave facilitated the crystalline phase formation. It was reported that the catalyst precipitated until the phase changing occurs (color change is observed) can provide relatively small catalyst crystallite size and high surface area [28]. Table 2 indicates that the surface acidity of the catalyst synthesized using ultrasonic-assisted method was higher than that of the conventional method. The catalyst dispersion was also improved as presented in Fig. 5. The ratio of Cu to Zn was 1.30 for conventional precipitation while it was 1.06, close to stoichiometric ratio (1:1 for Cu:Zn), for ultrasonic-assisted precipitation. From the reaction test, similar trends of methanol yield were obtained from both catalyst preparation methods, from which the yield increased as the precipitation temperature increased before decreasing after reaching its maximum as presented in Fig. 6. However, the maximum yield was obtained at 313 K for ultrasonic-assisted precipitation (32%) whereas it was at 333 K for conventional precipitation (31%). This indicated that although the methanol yield only slightly increased when ultrasonic irradiation was applied, the ultrasonic could help decrease the precipitation temperature of the catalyst. As presented in Table 1, an improved catalyst property was observed in 333 K_U sample, relatively more than 313 K_U sample but methanol yield decreased. However, an increase in CO_2 conversion was

observed, indicating a selectivity of the catalyst to by-products of the reaction. A correlation between an improved catalyst property on an increasing by-product selectivity (ethyl acetate) is not clear and require a further understanding to the mechanistic path of the reaction.

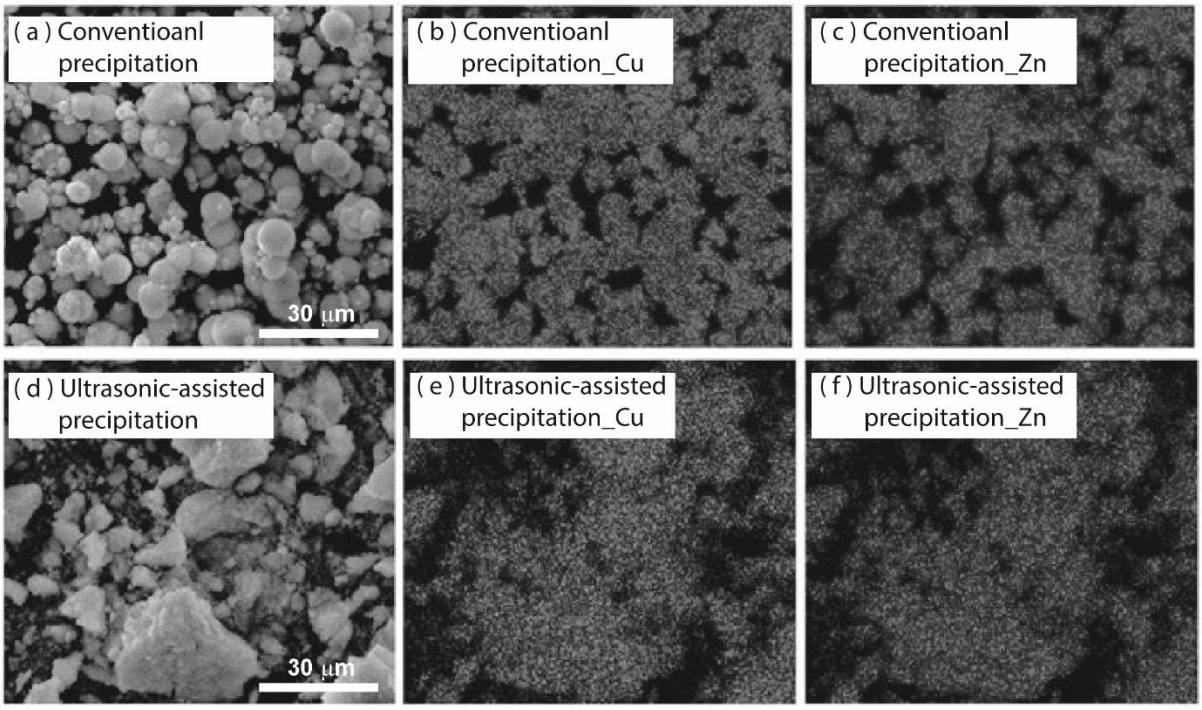

Figure 5 SEM-EDX images of the catalysts synthesized through a conventional precipitation and ultrasonic-assisted precipitation

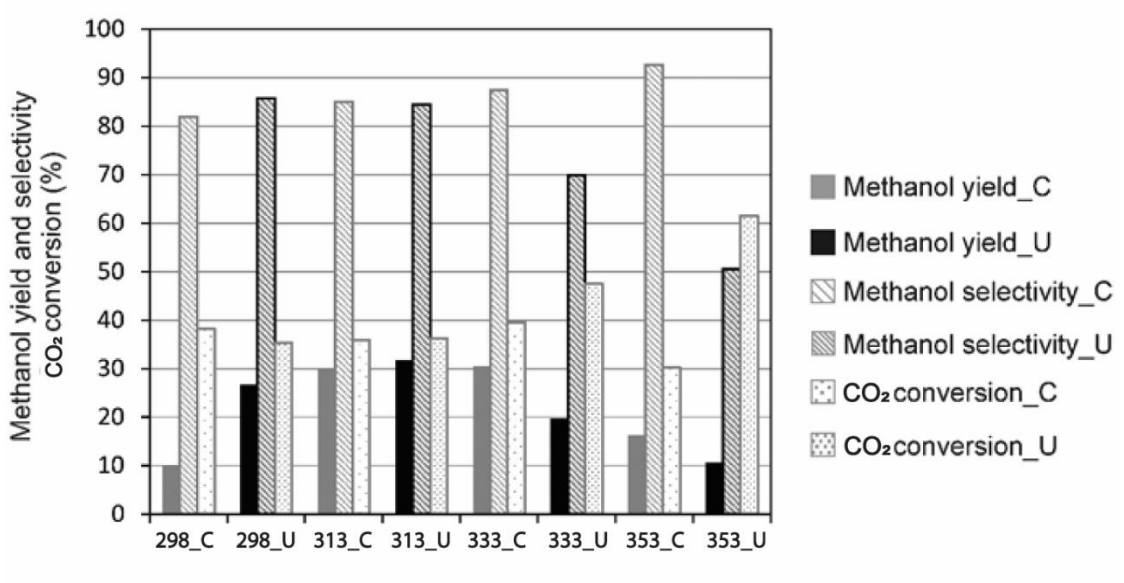

Figure 6 Yield and selectivity of methanol and CO_2 conversion using the catalysts synthesized through a conventional precipitation and ultrasonic-assisted precipitation at different temperatures (239-353 K), pH = 7 for all samples.

2.1.3.3 Research platform 2 - Effect of precipitation pH

Figure 2(c) presents the XRD patterns of CuO/ZnO synthesized using different pH values of mother liquor (pH 5-9) while the precipitating temperature was maintained at 333 K. The pH value during precipitation significantly affected the crystallite size of CuO and ZnO and precipitation at pH 8 provided the smallest crystallite size as presented in Table 1. All the samples exhibited similar XRD patterns, except the precipitation with pH 5. During the precipitation process at pH 5, the color change of mother liquor was not observed. The XRD peaks were relatively sharp and attained high intensity, indicating relatively large crystallite size.

The BET surface area was found to correlate with the catalyst crystallite size. The smaller crystal size provided the larger BET surface area and pore volume. The BET surface area and the pore volume interestingly increased when the pH increased and the largest BET surface area was obtained at pH 8 (90.67 m^2 g_{cat}^{-1}). In addition, the reducing temperature was decreased with pH value and again the lowest reducing temperature was obtained at pH 8, as shown in Table 1. The highest surface acidity (0.234 mmol NH_3 g_{cat}^{-1}) was also obtained at pH 8, as presented in Table 2. It was reported that pH value changes the growth of the species, leading to the formation of different crystal structures [44]. In this study, the dissolution of Cu^{2+} and Zn^{2+} ions from copper nitrate and zinc nitrate precursors as same as OH^- and CO^{3-} from Na_2CO_3 solution was believed to occur first. Then, the formation of precipitated product which can be a complex form of zinc-copper hydroxyl carbonate occurred. Varying pH value therefore affects the OH^- species and the formation of precipitated product.

Figure 7 exhibits the yield and selectivity of methanol and CO_2 conversion from the catalyst synthesized with different pH values. Methanol yield increased as increasing the pH value. The maximum methanol yield and CO_2 conversion was obtained at pH 8 (33% yield of methanol and 44% CO_2 conversion), where the CuO/ZnO catalyst exhibited relatively the highest surface acidity and the largest BET surface area. Methanol selectivity was 83% and the by-product was ethyl acetate and acetic acid. It was reported that ethyl acetate can be produced by catalytic dehydrogenation of ethanol [43].

It is worth discussing about possible products from alcohol-assisted method. Apart from methanol, a variety of ethyl acetate, methyl acetate, ethyl formate, and acetic were detected as by-products in previous works [11, 32, 38, 43]. Activated formate ($CHOO^-$) is an intermediate product from CO_2/H_2 reaction (Eq. (5)) before further reacting with H_2 to form methanol. However, it is possible that the activated formate reacts with ethanol (used in alcohol-assisted method) to generate ethyl acetate ($CH_3COOC_2H_5$) through dehydrogenation of alcohol over Cu/ZnO catalyst [38]. Therefore, alcohol used in this study (ethanol) acted as both medium and reaction intermediate in the case of ethyl acetate production. Methyl acetate can be formed after ethyl acetate reacts with methanol [11]. A further study is required to identify mechanistic path of methanol synthesis through the alcohol-assisted method. It is also of interest to control the product diversity through a control of operating conditions.

When comparing results from this work to those of Jeong et al. [32], although the CuO/ZnO from this work exhibits relatively much larger BET surface area, the methanol yield is relatively lower (33% in this work and above 45% from the work of Jeong et al.). This could be caused by difference in reactants, catalyst preparation, and reducing condition used. In detail, syngas was used as reactants in the work of Jeong et al. while CO_2/H_2 was applied in this work. In-situ catalyst reduction was used in this work while the work of Jeong applied ex-situ reduction which could be a preferable choice for further experiments. The relatively much higher surface area of the CuO/ZnO in this work was

likely due to low precipitation temperature which was found to have a significant impact on catalyst properties. Furthermore, the catalyst was precipitated at 333 K in this work while it was 343 K in the work of Jeong et al. [32].

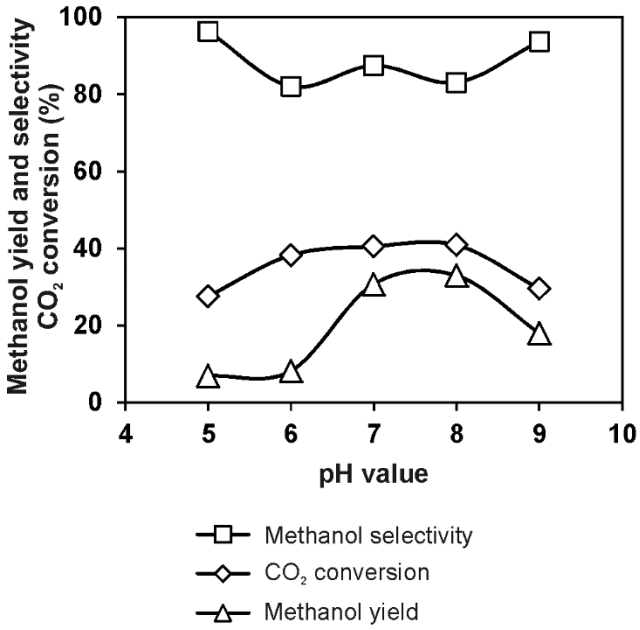

Figure 7 Yield and selectivity of methanol and CO_2 conversion using the catalysts precipitated at different pH (5-9)

2.1.3.4 Research platform 2 - Effect of alcohol type during alcohol-assisted methanol synthesis

During the alcohol-assisted methanol synthesis, alcohol was used as a medium. The effect of alcohol type was studied. Ethanol was replaced with propanol and butanol for methanol synthesis reaction and the results are shown in Fig. 8. Ethanol

provided the highest yield and selectivity of methanol, while the yield and selectivity decreased following the larger alcohol molecule. This was conflicting to the report that the electron density of oxygen atoms is higher in a larger alcohol molecule and hence promotes the ROH to react with the carbon atom of HCOOCu more quickly [19]. Acetate group was produced when the promoting alcohol was used as mentioned previously. The acetate compound is likely generated from a catalytic dehydrogenation of alcohol. Ethyl acetate, propyl acetate, and butyl acetate were detected when ethanol, propanol, and butanol were used as the promoting alcohol, respectively. It should be noted that acetic acid was slightly detected in the case of ethanol. It was likely that acetic acid further reacted with ethanol to produce ethyl acetate.

Although, the larger alcohol molecules exhibited lower yield and selectivity of methanol, it can be advantageous in term of purification unit after the reaction to separate methanol from alcohol medium since propanol and butanol have higher boiling point than ethanol. To improve the methanol yield while using large-molecule alcohol has become of interest.

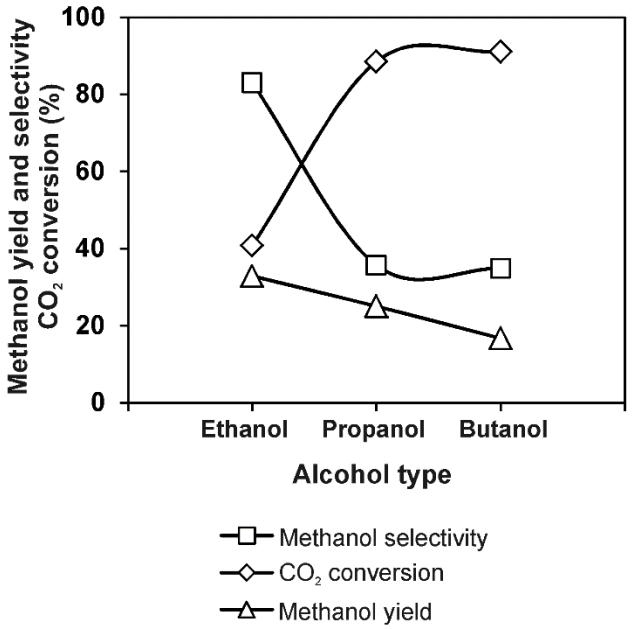

Figure 8 Yield and selectivity of methanol and CO_2 conversion when using different types of alcohol (ethanol, propanol and butanol)

2.1.4 Research platform 2 - Conclusions

In this study, CuO/ZnO catalysts were prepared using an ultrasonic-assisted precipitation and, methanol was synthesized through an alcohol-assisted method. The ultrasonic-assisted precipitation exhibited a potential to be applied for CuO/ZnO preparation while an alcohol-assisted method can be efficiently used for methanol synthesis. Preparation conditions significantly affected catalyst properties and activity during methanol synthesis. Although a further study to identify mechanistic path of methanol synthesis through the alcohol-assisted method, the catalyst properties such as smaller crystallite size, larger BET surface area, lower reducing temperature, and higher

surface acidity were related to an increase in yield and selectivity of methanol. Precipitation temperature significantly affected CuO/ZnO catalyst properties and methanol yield. The precipitation temperature could be decreased (from 333 K to 313 K) when ultrasonic was applied (50 W cm^{-2}). The ultrasonic-assisted precipitation method provided relatively larger surface area and well-dispersed catalyst, compared to conventional methods. Precipitating pH also affected the catalyst properties as well as the catalyst activity during methanol synthesis and pH 8 was found to be an optimal condition. From the reaction test, when the larger-molecule alcohol was used as a medium such as propanol and butanol, CO_2 conversion increased but the yield and selectivity of methanol decreased. Ethyl acetate, propyl acetate, and butyl acetate were obtained as by-products, depending on the alcohol type. It is therefore of challenge for future research to develop more suitable catalyst which offers high methanol yield when using a large-molecule alcohol for the alcohol-assisted methanol synthesis as it could offer a potential benefit in simplifying the subsequent product purification.

2.1.5 Research platform 2 - References

[1] EPA (US Environmental Protection Agency), Overview of Greenhouse Gases, Available at URL: https://www3.epa.gov/climatechange/ghgemissions/gases/co2.html. Acessed: 1st October 2017.

[2] Y. Santiago-Rodríguez, E. Barreto-Rodríguez, C.C.-A. MC, Journal of Molecular Catalysis A: Chemical 423 (2016) 319-332.

[3] S.S. Iyer, T. Renganathan, S. Pushpavanam, M.V. Kumar, N. Kaisare, Journal of CO_2 Utilization, 10 (2015) 95-104.

[4] H. Lei, R. Nie, G. Wu, Z. Hou, Fuel, 154 (2015) 161-166.

[5] L. Fan, V. Sakaiya, K. Fujimoto, Applied Catalysis A: General, 180 (1999) L11-13.

[6] R. Raudaskoski, M.V. Niemelae, R.L. Keiski, Topics in Catalysis, 45 (2007) 57-60.

[7] M. Asifa, X. Gao, H. LV, X. Xi, P. Dong, International Journal of Hydrogen Energy 43 (2018) 2726-2741.

[8] G.R. KaleBhaskar, D. Kulkarni, International Journal of Hydrogen Energy 38 (2013) 2624-2633.

[9] J.F. de la Fuente, S. H. Moreno, A. I. Stankiewicz, G. D. Stefanidis, International Journal of Hydrogen Energy 42 (2017) 12943-12955.

[10] A. I. Paksoy, B. S. Caglayan, E. Ozensoy, A.N. Ökte, A. E. Aksoylu, International Journal of Hydrogen Energy 43 (2018) 4321-4334.

[11] Y. Jeong, I. Kim, J.-Y. Kang, N. Yan, H. Jeong, J.-K. Park, H.-P. Park, J.-C. Jung., Journal of Molecular Catalysis A: Chemical, 418-419 (2016) 168-174

[12] N. Park, M.J. Park, Y.J. Lee, K.S. Ha, K.W. Jun, Fuel Processing Technology, 125 (2014) 139-147.

[13] B. Hu, Y. Yamaguchi, K. Fujimoto, Catalysis Communications, 10 (2009) 1620-1624.

[14] J. Sloczynski, R. Grabowski, P. Olszewski, A. Kozlowska, J. Stoch, M. Lachowska, Applied Catalysis A: General, 210 (2006) 127-137.

[15] H. Bahruji, M. Bowker, G. Hutchings, N. Dimitratos, P. Wells, E. Gibson, W. Jones, C. Brookes, D. Morgan, G. Lalev, Journal of catalysis, 343 (2016) 133-146.

[16] A.L. Valant, C. Comminges, C. Tisseraud, C. Canaff, L. Pinard, Y. Pouilloux, Journal of catalysis, 324 (2015) 41-49.

[17] S. Wesselbaum, V. Moha, M. Meuresch, S. Brosinski, K.M. Thenert, J. Kothe, T.V. Stein, U. Englert, M. Holscher, J. Klankermayer, W. Leitner, Chemical science, 6 (2015) 693-704.

[18] H. Arakawa, M. Aresa, J.N. Armor, M.A. Barteau, E.J. Beckman, E.T. Bell, Chemical Reviews, 101 (2001) 953-996.

[19] G.C. Chinchen, M.S. Spencer, K.C. Waugh, D.A. Whan, Journal of the chemical society faraday transactions : Physical chemistry in condensed phases, 83 (1987) 2193-2212.

[20] O.-S. Joo, K.-D. Jung, I. Moon, A.V. Rozovskii, G.I. Lin, S.H. Han, industrial and engineering chemistry research, 38 (1999) 1808-1812.

[21] G.C. Chinchen, M.S. Spencer, G.C. Chinchen, K.C. Waugh, D.A. Whan, Applied Catalysis A, 25 (1986) 101-107.

[22] M. Satio, K. Murata, Catalysis Surveys from Asia, 8 (2004) 285-294.

[23] J.Q. Zeng, N. Tsubaki, K. Fujimoto, Fuel, 81 (2002) 125-127.

[24] J. Wu, M. Satio, M. Takeuchi, T. Watanabe, Applied Catalysis A, 218 (2001) 235-240.

[25] R. Yang, Y. Fu, Y. Zhang, N. Tsubaki, Journal of catalysis., 228 (2004) 23-35.

[26] F. Meng, Q. Zhang, G. Yang, R. Yang, Y. Yoneyama, N. Tsubaki, Chemical engineering journal, 295 (2016) 160-166.

[27] I. Sharafutdinov, C.F. Elkjaer, W.P.D. Carvalho, D. Gardini, G.L. Chiarello, D.D. D, J.B. Wagner, J.D. Grunwaldt, S. Dahl, I. Chorkendorff, Journal of catalysis, 320 (2014) 77-88.

[28] J. Nerlov, I. Chorkendorff, Journal of catalysis, 181 (1999) 271-279.

[29] B.L. Kniep, F. Girgsdies, T. Ressler, Journal of catalysis, 236 (2005) 34-44.

[30] T. Xiao-bo, N. Tsubaki, X. Hong-juan, H. Yi-zhuo, T. Yi-sheng, Journal of fuel chemistry and technology, 42(6) (2014) 704-709.

[31] N. Tsubaki, M. Ito, K. Fujimoto, Journal of Catalysis, 197 (2001) 224-227.

[32] Y. Jeong, I. Kim, J.Y. Kang, H. Jeong, J.K. Park, J.H. Park, J.C. Jung, Journal of Molecular Catalysis A: Chemical, 400 (2015) 132–138.

[33] L. Shi, W. Shen, G. Yang, X. Fan, Y. Jin, X. Zeng, K. Matsuda, N. Tsubaki, Journal of Catalysis, 302 (2013) 83-90.

[34] X. Guo, D. Mao, G. Lu, S. Wang, G. Wu, Catalysis Communications, 12 (2011) 1095-1098.

[35] B.V. Farahani, F.H. Rajabi, M. Bahmani, M. Ghelichkhani, S. Sahebdelfar, Applied catalysis A: General, 482 (2014) 237-244.

[36] C. Tisseraud, C. Comminges, T. Belin, H. Ahouari, S. Soualah, Y. Pouilloux, A.L. Valant, Journal of Catalysis, 330 (2015) 533-544.

[37] S. Allahyari, M. Haghighi, A. Ebadi, S. Hosseinzadeh, Ultrasonics Sonochemistry, 21 (2014) 663-673.

[38] I. Kim, G. Lee, H. Jeong, J.H. Park, J.C. Jung, Journal of Energy Chemistry, 26 (2017) 373-379.

[39] S.A. Kondrat, P.J. Smith, P.P. Wells, P.A. Chater, J.H. Carter, D.J. Morgan, E.M. Fiordaliso, J.B. Wagner, T.E. Davies, L. Lu, J.K. Bartley, S.H. Taylor, M.S. Spencer, C.J. Kiely, G.J. Kelly, C.W. Park, M.J. Rosseinsky, G.J. Hutchings, Nature, 531 (2016) 83-87.

[40] M. Behrens, F. Girgsdies, A. Trunschke, R. Schlögl, European Journal of Inorganic Chemistry, 2009 (2009) 1347-1357.

[41] X. Jiang, N. Koizumi, X, Guo, C, Song, Applied Catalysis B: Environmental, 170-171 (2015) 173-185.

[42] F. Meshkini, M. Taghizadeh, M. Bahmani, Fuel 89 (2010) 170–175.

[40] E.N. Muhamad, R. Irmawati, Y.H. Taufiq-Yap, A.H. Abdullah, B.L. Kniep, F. Girgsdies, T. Ressler, Catalysis today, 131 (2008) 118-124.

[43] E. Santacesaria, G. Carotenuto, R. Tesser, M.D. Serio, Chemical Engineering Journal, 179 (2012) 209-220.

[44] H. Kiani, D-W. Sun, Z. Zhang, Ultrasonics Sonochemistry, 19 (2012) 1238-1245.

Appendix – publications

Publication 1

Fuel Processing Technology 173 (2018) 119–125

Contents lists available at ScienceDirect

Fuel Processing Technology

journal homepage: www.elsevier.com/locate/fuproc

Research article

Effect of sintering additives on barium cerate based solid oxide electrolysis cell for syngas production from carbon dioxide and steam

S. Likhittaphon[a], T. Pukkrueapun[a], P. Seeharaj[b], U. Wetwathana Hartley[c], N. Laosiripojana[d], P. Kim-Lohsoontorn[a,c,*]

[a] Department of Chemical Engineering, Mahidol University, Nakorn Pathom 73170, Thailand
[b] Department of Chemistry, King Mongkut's Institute of Technology Ladkrabang, Bangkok 10520, Thailand
[c] The Sirindhorn International Thai-German Graduate School of Engineering, King Mongkut's University of Technology North Bangkok, Bangkok 10800, Thailand
[d] The Joint Graduate School of Energy and Environment, King Mongkut's University of Technology Thonburi, Bangkok 10140, Thailand
[e] Department of Chemical Engineering, Chulalongkorn University, Bangkok 13300, Thailand

ARTICLE INFO

Keywords:
Proton conductor
Sintering additive
Solid oxide electrolysis cell
Carbon dioxide utilization
Syngas production

ABSTRACT

The effect of sintering additives (NiO, Co_2O_3, and ZnO) on the performance of barium-cerate-based solid oxide electrolysis cell (SOEC) is investigated. The performance of the SOEC with different sintering additives is determined in terms of relative density, electrochemical performance, and catalytic activity toward reverse water gas shift reaction. $BaCeO_3$ (BC) and $BaCe_{0.9}Gd_{0.1}O_{3-\delta}$ (BCG) are synthesized using conventional precipitation method, comparing to ultrasonic-assisted precipitation. The sintering additives promote both densification and grain growth. The relative density of the BCG without sintering additive is 69% while that of the BCG with 1 wt% of Co_2O_3, NiO and ZnO is 95%, 95% and 88%, respectively. The SEM images indicate that the BCG with sintering additives exhibits dense grains with relatively large grain size. Although the BGC with NiO and Co_2O_3 exhibit maximum relative density, the sample with ZnO shows relatively highest conductivity with the lowest activation energy of conduction and the sample with NiO provides the largest CO yield and CO_2 conversion. The activation energy of conduction is found to be 375.41, 70.06, 66.86 and 61.80 kJ mol^{-1} for BCG, BCG with 1 wt% Co_2O_3, NiO and ZnO, respectively. The BCG with 1 wt% NiO provides the highest CO_2 conversion and CO yield at temperature below 700 °C (62% CO_2 conversion and 32% CO yield at 700 °C). Temperature program of oxidation (TPO) reveals that carbon deposition can cause the low CO yield at the operating temperature above 700 °C.

1. Introduction

Solid oxide electrolysis cells (SOECs) are considered as promising system for H_2 and syngas production from steam and carbon dioxide through steam electrolysis application coupling reverse water gas shift reaction, as shown in Eqs. (1)-(4).

Steam electrolysis: $H_2O \rightarrow H_2 + 0.5O_2$ (1)

Anode: $H_2O \rightarrow 2H^+ + 2e^- + 0.5O_2$ (2)

Cathode: $2H^+ + 2e^- \rightarrow 0.5H_2$ (3)

Reverse water gas shift: $H_2 + CO_2 \leftrightarrow CO + H_2O$ (4)

Conventional SOECs consist of oxide ion (O^{2-}) conducting electrolyte such as yttria stabilised zirconia (YSZ) or doped ceria [1–6]. However, proton (H^+) conducting electrolyte has received considerable attention for an application in SOEC [7,8]. Due to its much smaller ionic radius, proton mobility is theoretically faster than oxygen-ion [7]. Among the ABO_3 perovskite-type proton-conductor, $BaCeO_3$ exhibits relatively high conductivity (0.04 S cm^{-1} at 600 °C) [9]. However, barium cerate cannot be easily densified at low temperature. High sintering temperature (1500–1700 °C) is required to obtain a relative density above 90% [10,11]. This leads to issues relating the cell fabrication process; insufficient density of the cell; and, high sintering temperature. Low cell density leads to poor conductivity and gas leakage while high sintering temperature can cause undesired phases and poor chemical homogeneity. The evaporation of BaO can occur at temperature above 1550 °C [12].

Sinterability of polycrystalline ceramics mainly depends on mass transport diffusion mechanism which can be controlled by temperature, time, the size of starting powder, and the addition of sintering aid [1,13,14]. Small amounts of transition metal (e.g. Cu, Ni, Fe, Co) have been reported to enhance sinterability of the materials [15–23]. The gadolinium doped barium cerate co-doped by small amounts of

* Corresponding author.
E-mail address: pattaraporn.k@chula.ac.th (P. Kim-Lohsoontorn).

https://doi.org/10.1016/j.fuproc.2018.01.019
Received 30 November 2017; Received in revised form 22 January 2018; Accepted 23 January 2018
Available online 03 February 2018

Publication 2

ELSEVIER

Log In Register Help

Track Your Accepted Article

The easiest way to check the publication status of your accepted article

Effect of CuO/ZnO catalyst preparation condition on alcohol-assisted methanol synthesis from carbon dioxide and hydrogen

Article reference	HE23853
Journal	International Journal of Hydrogen Energy
Corresponding author	P. Kim-Lohsoontorn
First author	S. Likhittaphon
Received at Editorial Office	20 Apr 2018
Article revised	18 Jun 2018
Article accepted for publication	4 Jul 2018

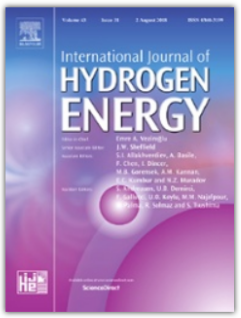

ISSN 0360-3199

Last update: 23 Jul 2018

Share via email

Feedback

ARTICLE IN PRESS

INTERNATIONAL JOURNAL OF HYDROGEN ENERGY XXX (2018) 1–10

Available online at www.sciencedirect.com

ScienceDirect

journal homepage: www.elsevier.com/locate/he

Effect of CuO/ZnO catalyst preparation condition on alcohol-assisted methanol synthesis from carbon dioxide and hydrogen

S. Likhittaphon [a], R. Panyadee [a], W. Fakyam [a], S. Charojrochkul [b], T. Sornchamni [c], N. Laosiripojana [d], S. Assabumrungrat [e], P. Kim-Lohsoontorn [e,*]

[a] Department of Chemical Engineering, Mahidol University, Nakhon Pathom, 73170, Thailand
[b] National Metal and Materials Technology Center (MTEC), National Science and Technology Development Agency (NSTDA), Pathumtani, 12120, Thailand
[c] PTT Research & Technology Institute, PTT Public Company Limited, Bangkok, 13170, Thailand
[d] The Joint Graduate School of Energy and Environment, King Mongkut's University of Technology Thonburi, Bangkok, 10140, Thailand
[e] Center of Excellence in Catalysis and Catalytic Reaction Engineering, Department of Chemical Engineering, Faculty of Engineering, Chulalongkorn University, Bangkok, 10330, Thailand

ARTICLE INFO

Article history:
Received 20 April 2018
Received in revised form
18 June 2018
Accepted 4 July 2018
Available online xxx

Keywords:
Alcohol-assisted methanol synthesis
Ultrasonic-assisted precipitation
CO_2 utilization
Methanol synthesis
Copper zinc oxide

ABSTRACT

CuO/ZnO catalysts are synthesized using a co-precipitation method with different precipitation temperatures (298–353 K) and pH values (5–9). A conventional precipitation is compared to an ultrasonic-assisted precipitation at each precipitating temperature. Methanol is directly synthesized from CO_2 and H_2 (1:3 mol ratio) through an alcohol-assisted reaction (423 K, 5 MPa, 24 h) by using different alcohols (ethanol, propanol and butanol) as a medium. There are two parts for the challenge of this research, including the preparation of CuO/ZnO catalysts using an ultrasonic-assisted precipitation and, methanol synthesis through an alcohol-assisted method. It is found that the precipitation temperature and pH value significantly affect the catalyst properties and the reaction activity. An ultrasonic irradiation helps facilitate the crystalline phase formation and decrease precipitation temperature. The highest yield of methanol is obtained when CuO/ZnO is precipitated at 333 K from the conventional precipitation (31%) while it is at 313 K from the ultrasonic-assisted precipitation (32%). In addition, the different type of alcohol strongly affects methanol yield and CO_2 conversion. The use of larger alcohol molecules offers higher CO_2 conversion but lower methanol yield.

Introduction

Fossil fuel is commonly used as a major energy supply, which is also a main source of CO_2 emission [1–5]. Currently, CO_2 emission is 6.2 million tons per year, and tends to increase each year. The increasing CO_2 concentration in atmosphere was predicted to be 44% from 2006 to 2030 [6]. Carbon capture and sequestration (CCS) has been proposed as a strategy to

* Corresponding author.
E-mail address: pattarapom.k@chula.ac.th (P. Kim-Lohsoontorn).
https://doi.org/10.1016/j.ijhydene.2018.07.021

Publication 3

ELSEVIER

Log In Register Help

Track Your Accepted Article

The easiest way to check the publication status of your accepted article

Effect of strontium and zirconium doped barium cerate on the performance of proton ceramic electrolyser cell for syngas production from carbon dioxide and steam

Article reference	HE23953
Journal	International Journal of Hydrogen Energy
Corresponding author	Pattaraporn Kim-Lohsoontorn
First author	J. Sarabut
Received at Editorial Office	30 Apr 2018
Article revised	15 Jul 2018
Article accepted for publication	18 Jul 2018

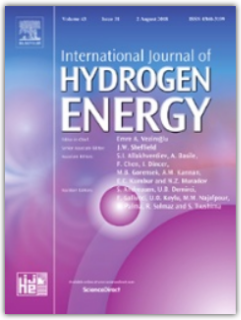

ISSN 0360-3199

Last update: 23 Jul 2018

Share via email

Feedback